Self-assembly of new porous materials

by

Tia Jacobs

Submitted in partial fulfilment of the requirements for the degree

Doctor of Philosophy

at

Stellenbosch University

Department of Chemistry and Polymer Science

Faculty of Science

Supervisor: Prof. L. J. Barbour

Co-Supervisor: Dr. M. W. Bredenkamp

Date: March 2009

Table 4.1 Electron counts, occupancies and structural parameters of **15** with included methanol (**15$_{MeOH}$**), desolvated under ambient conditions (**15**) and under vacuum (**15$_{vac}$**). Volumes are calculated with r_{probe} = 1.4 Å and the methanol atoms are labeled C17**–**O18**–**H18.

	15$_{MeOH}$	**15**	**15$_{vac}$**
Pressure (bar)	1	1	0
Temperature (°C)	-173	22	22
Void volume (Å^3)	131	-	117
Electron count	33.0	3.8	0
Occupancy (%)	91.7	11	0
Cell length *a* (Å)	17.208(2)	18.128(6)	18.200(3)
Cell length *b* (Å)	15.593(2)	15.613(4)	15.525(2)
Cell length *c* (Å)	9.6635(9)	9.372(3)	9.361(1)
Cell angle β (º)	114.257	114.658	115.029
Cell volume (Å^3)	2363.95	2410.57	2396.56
Cd1–N4 (Å)	2.206(3)	2.213(4)	2.227(5)
Cd1–Cl3 (Å)	2.449(1)	2.415(2)	2.411(2)
Cd1–Cl2 (Å)	2.443(1)	2.438(2)	2.435(2)
Cd1^{i}···Cd1^{iv} (Å)	8.5034(9)	8.738(2)	8.695(2)
Cd1^{iii}···Cd1^{iv} (Å)	8.543(1)	9.373(3)	9.444(2)
Cd1^{i}···Cd1^{vi} (Å)	16.075(2)	15.508(5)	15.403(3)
Cd1^{ii}···Cd1^{iii} (Å)	16.138(1)	16.584(4)	16.674(2)
Cd1^{ii}···Cd1^{v} (Å)	25.192(2)	25.256(6)	25.339(3)
Cl3^{i}···Cl3^{iv} (Å)	4.433(3)	5.795(6)	5.726(7)
Cl3^{i}···Cl3^{vi} (Å)	11.226(3)	10.717(5)	10.611(5)
Cl3^{iii}···Cl3^{iv} (Å)	10.003(3)	11.312(6)	11.323(6)
Cl3···O18 (Å)	3.175(5)	-	-
Cl3···H18 (Å)	2.34(3)	-	-
∠Cl3···H18–O18 (º)	173.7	-	-
C17···C17 (Å)	3.82(1)	-	-

Symmetry codes: (i) –x, y, 2-z; (ii) x, y, 1+z; (iii) –x, y, 3-z; (iv) x, y, 2+z; (v) –x, y, 4-z; (vi) x, y, 3+z.

Table 4.2 Electron counts, occupancies and structural parameters of **15** under various C_2H_2 pressures. Volumes are calculated with r_{probe} = 1.4 Å and the atoms of the guest C_2H_2 molecule are labeled H17–C17≡C18–H18.

	$15_{05,C2H2}$	**$15_{1,C2H2}$**	**$15_{2,C2H2}$**	**$15_{4,C2H2}$**	**$15_{6,C2H2}$**	**$15_{8,C2H2}$**	**$15_{16,C2H2}$**
C_2H_2 pressure (bar)	0.5	1	2	4	6	8	16
Temperature (°C)	22	22	22	22	22	22	22
Void volume (Å^3)	-	-	135	-	-	-	146
Electron count	10.1	13.2	14.8	21.3	23.3	24.3	25.3
Occupancy (%)	36.1	47.1	52.9	76.1	83.2	86.8	90.4
Cell length *a* (Å)	18.024(3)	17.901(2)	17.788(3)	17.457(5)	17.307(3)	17.268(3)	17.285(5)
Cell length *b* (Å)	15.608(2)	15.618(2)	15.640(2)	15.626(5)	15.620(3)	15.611(3)	15.604(5)
Cell length *c* (Å)	9.424(1)	9.447(1)	9.506(1)	9.708(3)	9.814(2)	9.850(2)	9.858(3)
Cell angle β (º)	114.506	114.303	114.143	113.570	113.471	113.428	113.327
Cell volume (Å^3)	2412.26	2407.18	2413.24	2427.08	2433.56	2436.21	2441.63
Cd1–N4 (Å)	2.222(4)	2.218(4)	2.231(5)	2.219(7)	2.225(5)	2.225(4)	2.235(6)
Cd1–Cl3 (Å)	2.417(2)	2.419(3)	2.423(3)	2.408(5)	2.410(3)	2.410(3)	2.409(4)
Cd1–Cl2 (Å)	2.441(2)	2.440(2)	2.433(2)	2.442(4)	2.439(3)	2.441(3)	2.439(4)
Cd1^{i}···Cd1^{iv} (Å)	8.740(1)	8.727(1)	8.725(2)	8.790(3)	8.816(3)	8.830(3)	8.862(3)
Cd1^{iii}···Cd1^{iv} (Å)	9.267(2)	9.160(1)	9.101(2)	8.737(3)	8.612(3)	8.578(3)	8.586(3)
Cd1^{i}···Cd1^{vi} (Å)	15.636(2)	15.713(2)	15.817(3)	16.331(6)	16.550(3)	16.625(4)	16.666(5)
Cd1^{ii}···Cd1^{iii} (Å)	16.522(2)	16.436(2)	16.440(2)	16.244(4)	16.224(3)	16.224(3)	16.226(4)
Cd1^{ii}···Cd1^{v} (Å)	25.253(3)	25.197(3)	25.268(3)	25.295(7)	25.395(4)	25.434(4)	25.440(6)
Cl3^{i}···Cl3^{iv} (Å)	5.712(6)	5.658(7)	5.525(8)	5.23(1)	5.10(1)	5.07(1)	5.08(1)
Cl3^{i}···Cl3^{vi} (Å)	10.834(5)	10.906(6)	10.988(7)	11.52(1)	11.74(1)	11.81(1)	11.85(1)
Cl3^{iii}···Cl3^{iv} (Å)	11.202(6)	11.116(7)	11.003(8)	10.51(1)	10.34(1)	10.29(1)	10.28(1)
Cl3···C18 (Å)	-	-	3.51(5)	-	-	-	3.41(3)
C17···C17 (Å)	-	-	1.74(8)	-	-	-	3.19(5)
C17···H17 (Å)	-	-	1.05	-	-	-	2.72
∠Cl3···C18–C17 (º)	-	-	172.84	-	-	-	151.72
∠Cd1–Cl3···C18 (º)	-	-	176.41	-	-	-	177.29

Symmetry codes: (i) –x, y, 2-z; (ii) x, y, 1+z; (iii) –x, y, 3-z; (iv) x, y, 2+z; (v) –x, y, 4-z; (vi) x, y, 3+z.

Table 4.3 Electron counts, occupancies and structural parameters of **15** under various CO_2 pressures. Volumes are calculated with r_{probe} = 1.4 Å and the atoms of the guest CO_2 molecule are labeled O18–C17–O19.

	$15_{05,CO2}$	**$15_{1,CO2}$**	**$15_{2,CO2}$**	**$15_{4,CO2}$**	**$15_{6,CO2}$**
CO_2 pressure (bar)	0.5	1	2	4	6
Temperature (°C)	22	22	22	22	22
Void volume (Å^3)	-	-	-	-	-
Electron count	15.0	16.2	22.2	22.7	25.7
Occupancy (%)	34.1	36.8	50.5	51.6	58.4
Cell length *a* (Å)	18.046(2)	18.033(2)	18.030(2)	18.009(2)	18.028(2)
Cell length *b* (Å)	15.525(2)	15.535(1)	15.535(2)	15.546(2)	15.537(2)
Cell length *c* (Å)	9.394(1)	9.3977(8)	9.400(1)	9.403(1)	9.409(1)
Cell angle β (º)	114.539	114.501	114.450	114.383	114.365
Cell volume (Å^3)	2394.21	2395.62	2396.87	2397.87	2400.88
Cd1–N4 (Å)	2.226(3)	2.225(3)	2.224(4)	2.224(3)	2.222(3)
Cd1–Cl3 (Å)	2.415(2)	2.418(2)	2.417(2)	2.417(2)	2.416(2)
Cd1–Cl2 (Å)	2.437(2)	2.436(1)	2.441(2)	2.437(2)	2.439(2)
Cd1^{i}···Cd1^{iv} (Å)	8.746(1)	8.750(1)	8.757(1)	8.762(1)	8.774(1)
Cd1^{iii}···Cd1^{iv} (Å)	9.342(1)	9.331(1)	9.323(1)	9.309(1)	9.318(1)
Cd1^{i}···Cd1^{vi} (Å)	15.564(2)	15.579(2)	15.595(2)	15.613(2)	15.627(2)
Cd1^{ii}···Cd1^{iii} (Å)	16.569(1)	16.560(1)	16.549(2)	16.534(1)	16.546(1)
Cd1^{ii}···Cd1^{v} (Å)	25.264(2)	25.259(2)	25.250(2)	25.237(2)	25.254(2)
Cl3^{i}···Cl3^{iv} (Å)	5.812(5)	5.822(5)	5.852(6)	5.857(5)	5.872(6)
Cl3^{i}···Cl3^{vi} (Å)	10.777(4)	10.788(4)	10.813(5)	10.831(4)	10.849(4)
Cl3^{iii}···Cl3^{iv} (Å)	11.310(5)	11.316(5)	11.328(6)	11.320(5)	11.329(6)
Cl3···C17 (Å)	-	-	-	-	-
∠Cl3···C17–O18 (º)	-	-	-	-	-
∠Cl3···C17–O19 (º)	-	-	-	-	-
∠Cd1–Cl3···C17 (º)	-	-	-	-	-
C17···O18 (Å)	-	-	-	-	-

Symmetry codes: (i) –x, y, 2-z; (ii) x, y, 1+z; (iii) –x, y, 3-z; (iv) x, y, 2+z; (v) –x, y, 4-z; (vi) x, y, 3+z.

Table 4.3 Continued.

	$\mathbf{15}_{8,CO2}$	$\mathbf{15}_{10,CO2}$	$\mathbf{15}_{12,CO2}$	$\mathbf{15}_{14,CO2}$	$\mathbf{15}_{CO2}$
CO_2 pressure (bar)	8	10	12	14	10
Temperature (°C)	22	22	22	22	-40
Void volume (Å^3)	-	-	-	-	145
Electron count	27.2	27.8	28.0	28.5	43.4
Occupancy (%)	61.8	63.2	63.6	64.8	98.6
Cell length *a* (Å)	18.025(2)	18.026(2)	18.041(3)	18.029(2)	17.993(2)
Cell length *b* (Å)	15.543(1)	15.550(1)	15.535(3)	15.542(2)	15.479(2)
Cell length *c* (Å)	9.410(1)	9.411(1)	9.411(2)	9.411(1)	9.423(1)
Cell angle β (º)	114.31	114.28	114.28	114.25	114.12
Cell volume (Å^3)	2402.60	2404.70	2404.41	2404.32	2395.43
Cd1–N4 (Å)	2.220(3)	2.220(3)	2.217(3)	2.219(3)	2.217(4)
Cd1–Cl3 (Å)	2.417(2)	2.417(2)	2.417(2)	2.418(2)	2.424(2)
Cd1–Cl2 (Å)	2.441(1)	2.440(1)	2.442(2)	2.439(1)	2.450(2)
Cd1^{i}···Cd1^{iv} (Å)	8.780(1)	8.787(1)	8.792(1)	8.793(1)	8.769(1)
Cd1^{iii}···Cd1^{iv} (Å)	9.313(1)	9.309(1)	9.317(2)	9.310(1)	9.278(2)
Cd1^{i}···Cd1^{vi} (Å)	15.638(2)	15.649(2)	15.650(3)	15.656(2)	15.662(2)
Cd1^{ii}···Cd1^{iii} (Å)	16.536(1)	16.531(1)	16.537(2)	16.529(1)	16.519(2)
Cd1^{ii}···Cd1^{v} (Å)	25.243(2)	25.239(2)	25.244(3)	25.236(2)	25.244(3)
Cl3^{i}···Cl3^{iv} (Å)	5.884(5)	5.893(5)	5.893(5)	5.890(5)	5.929(6)
Cl3^{i}···Cl3^{vi} (Å)	10.860(4)	10.872(4)	10.872(4)	10.875(4)	10.883(5)
Cl3^{iii}···Cl3^{iv} (Å)	11.330(5)	11.332(5)	11.331(5)	11.326(5)	11.378(5)
Cl3···C17 (Å)	-	-	-	-	3.38(2)
∠Cl3···C17–O18 (º)	-	-	-	-	95.71
∠Cl3···C17–O19 (º)	-	-	-	-	88.60
∠Cd1–Cl3···C17 (º)	-	-	-	-	165.14
C17···O18 (Å)	-	-	-	-	4.04(3)

Symmetry codes: (i) –x, y, 2-z; (ii) x, y, 1+z; (iii) –x, y, 3-z; (iv) x, y, 2+z; (v) –x, y, 4-z; (vi) x, y, 3+z.

Table 4.4 Electron counts, occupancies and structural parameters of **16**$_{CH2Cl2}$, **16**$_{vac}$ and **16** under various CO_2 pressures. **16**$_{CO2}$ (last column) is the structure determined at 10 bar and 233 K. Volumes are calculated with r_{probe} = 1.4 Å and the atoms of the guest CO_2 molecule are labeled C17–O18.

	16$_{CH2Cl2}$	**16**$_{vac}$	**16**$_{1,CO2}$	**16**$_{2,CO2}$	**16**$_{4,CO2}$
CO_2 pressure (bar)	1	0	1	2	4
Temperature (°C)	-173	22	22	22	22
Void volume (Å^3)	133	124	-	-	-
Electron count	36.6	0.6	13.6	15.9	18.3
Occupancy (%)	87.1	1.4	30.9	36.1	41.6
Cell length *a* (Å)	17.799(1)	18.082(2)	17.993(3)	17.996(2)	17.985(2)
Cell length *b* (Å)	16.188(2)	16.339(2)	16.319(2)	16.317(2)	16.306(2)
Cell length *c* (Å)	9.416(1)	9.322(1)	9.366(1)	9.377(1)	9.376(1)
Cell angle β (º)	113.843	113.58	113.60	113.63	113.58
Cell volume (Å^3)	2481.62	2523.64	2520.08	2522.69	2519.98
Cd1–N4 (Å)	2.24(1)	2.235(6)	2.244(6)	2.247(6)	2.244(6)
Cd1–I3 (Å)	2.736(1)	2.736(1)	2.733(1)	2.732(1)	2.731
Cd1–I2 (Å)	2.735(2)	2.718(1)	2.725(1)	2.725(1)	2.725(1)
Cd1^{i}···Cd1^{iv} (Å)	8.771(2)	8.887(2)	8.866(2)	8.869(2)	8.873(2)
Cd1^{iii}···Cd1^{iv} (Å)	8.971(3)	9.145(2)	9.081(2)	9.087(2)	9.080(2)
Cd1^{i}···Cd1^{vi} (Å)	15.834(3)	15.753(2)	15.817(3)	15.831(2)	15.839(2)
Cd1^{ii}···Cd1^{iii} (Å)	16.166(3)	16.188(2)	16.180(2)	16.197(2)	16.185(2)
Cd1^{ii}···Cd1^{v} (Å)	24.891(4)	24.785(3)	24.830(3)	24.859(3)	24.846(3)
I3^{i}···I3^{iv} (Å)	5.561(3)	5.737(2)	5.651(2)	5.653(2)	5.657(2)
I3^{i}···I3^{vi} (Å)	10.426(3)	10.357(2)	10.415(2)	10.431(2)	10.441(2)
I3^{iii}···I3^{iv} (Å)	11.423(3)	11.505(2)	11.438(2)	11.444(2)	11.437(2)
I3···C17 (Å)	-	-	-	-	-
∠I3···O18–C17 (º)	-	-	-	-	-
∠Cd1–I3···O18 (º)	-	-	-	-	-

Symmetry codes: (i) –x, y, 2-z; (ii) x, y, 1+z; (iii) –x, y, 3-z; (iv) x, y, 2+z; (v) –x, y, 4-z; (vi) x, y, 3+z.

Table 4.4 Continued

	$\mathbf{16}_{8,CO2}$	$\mathbf{16}_{12,CO2}$	$\mathbf{16}_{16,CO2}$	$\mathbf{16}_{19,CO2}$	$\mathbf{16}_{CO2}$
CO_2 pressure (bar)	8	12	16	19	10
Temperature (°C)	22	22	22	22	-40
Void volume (Å^3)	-	-	126	-	
Electron count	20.2	21.4	22.3	22.7	25.9
Occupancy (%)	45.9	48.6	50.7	51.6	59
Cell length *a* (Å)	17.993(2)	18.000(3)	18.003(2)	17.996(3)	18.005(2)
Cell length *b* (Å)	16.295(2)	16.305(2)	16.305(2)	16.297(2)	16.271(2)
Cell length *c* (Å)	9.383(1)	9.393(1)	9.393(1)	9.389(1)	9.394(1)
Cell angle β (º)	113.534	113.50	113.47	113.52	113.38
Cell volume (Å^3)	2522.29	2527.93	2529.00	2525.00	2526.13
Cd1–N4 (Å)	2.241(6)	2.244(6)	2.238(6)	2.248(9)	2.237(6)
Cd1–I3 (Å)	2.732(1)	2.735(1)	2.733(1)	2.731(2)	2.736(1)
Cd1–I2 (Å)	2.725(1)	2.726(1)	2.725(1)	2.723(2)	2.729(1)
Cd1^{i}···Cd1^{iv} (Å)	8.889(2)	8.903(2)	8.911(2)	8.908(2)	8.952(2)
Cd1^{iii}···Cd1^{iv} (Å)	9.087(2)	9.093(2)	9.096(2)	9.094(3)	9.124(2)
Cd1^{i}···Cd1^{vi} (Å)	15.860(3)	15.884(3)	15.890(2)	15.884(3)	15.922(3)
Cd1^{ii}···Cd1^{iii} (Å)	16.193(2)	16.203(2)	16.203(2)	16.197(3)	16.213(2)
Cd1^{ii}···Cd1^{v} (Å)	24.859(3)	24.876(3)	24.875(3)	24.866(4)	24.879(3)
I3^{i}···I3^{iv} (Å)	5.669(2)	5.679(2)	5.692(2)	5.693(3)	5.841(2)
I3^{i}···I3^{vi} (Å)	10.462(2)	10.480(2)	10.491(2)	10.489(3)	10.543(2)
I3^{iii}···I3^{iv} (Å)	11.442(2)	11.451(2)	11.453(2)	11.450(3)	11.557(2)
I3···C17 (Å)	-	-	5.246(1)	-	
∠I3···O18–C17 (º)	-	-	174.09	-	
∠Cd1–I3···O18 (º)	-	-	170.35	-	

Symmetry codes: (i) –x, y, 2-z; (ii) x, y, 1+z; (iii) –x, y, 3-z; (iv) x, y, 2+z; (v) –x, y, 4-z; (vi) x, y, 3+z.

4.2.4 Gas sorption: a gravimetric study of 15-17

The three isostructural metallocycles **15-17** were prepared using **L** and different CdX_2 metal salts (X = Cl, Br or I). As shown in Figure 4.17, the shapes and sizes of the cavities are quite similar, and it should be noted that the size of the anion does not seem to influence the accessible void volume significantly. It was of interest to determine what, if any, effect substitution of the anion would have upon the guest sorption behaviour of the different materials. To this end the gas sorption abilities of **15-17** towards CO_2 and N_2 were investigated at various temperatures using gravimetric gas sorption methods. A range of experiments were conducted and, under the conditions used, the different compounds all exhibit Type I sorption behaviour (sorption isotherms are given in Figure 4.29 and Figure 4.30). From these experiments it is apparent that the chloride-containing metallocycle (**15**) absorbs better than the bromide-containing metallocycle (**17**) which absorbs better than the iodide-containing metallocycle (**16**). It was initially thought that these sorption experiments would reveal information about the role of the electrostatic profile of the host ions surrounding the voids with regard to the gas sorption ability of the material. Iodine is the largest and the less electronegative of the halogens investigated, and also the least reactive. Chlorine, on the other hand, is smaller and far more electronegative. However, besides forming part of the cavity wall, the two halide ions also form the gates between two neighbouring cavities. As previously described (with reference to Figure 4.6), anions of metallocycles 1 and 4 form the ceiling and floor of one cavity. Entry into this cavity is guarded on the left by anions of metallocycles 1 and 3, and on the right by anions of metallocycles 2 and 4. In the vacuum structures of **15-17**, the $X^-\cdots X^-$ distances across the entrance of the cavity are roughly equivalent to one another, with $Cl3^{i}\cdots Cl3^{iv}$ = 5.770(5), $Br3^{i}\cdots Br3^{iv}$ = 5.726(2) and $I3^{i}\cdots I3^{iv}$ = 5.737(2) Å (Figure 4.28). Hence, as the van der Waals radius of the halogen increases, the pore leading into the cavity becomes smaller. Thus an investigation of the influence of the electrostatic profile of the cavity on guest sorption ability is complicated by the fact that *two* parameters are changed with substitution of the halogen counter ion, *i.e.* (i) electrostatic profile of the internal void surface and (ii) gate size. However, all of these metallocycles were originally obtained as solvates

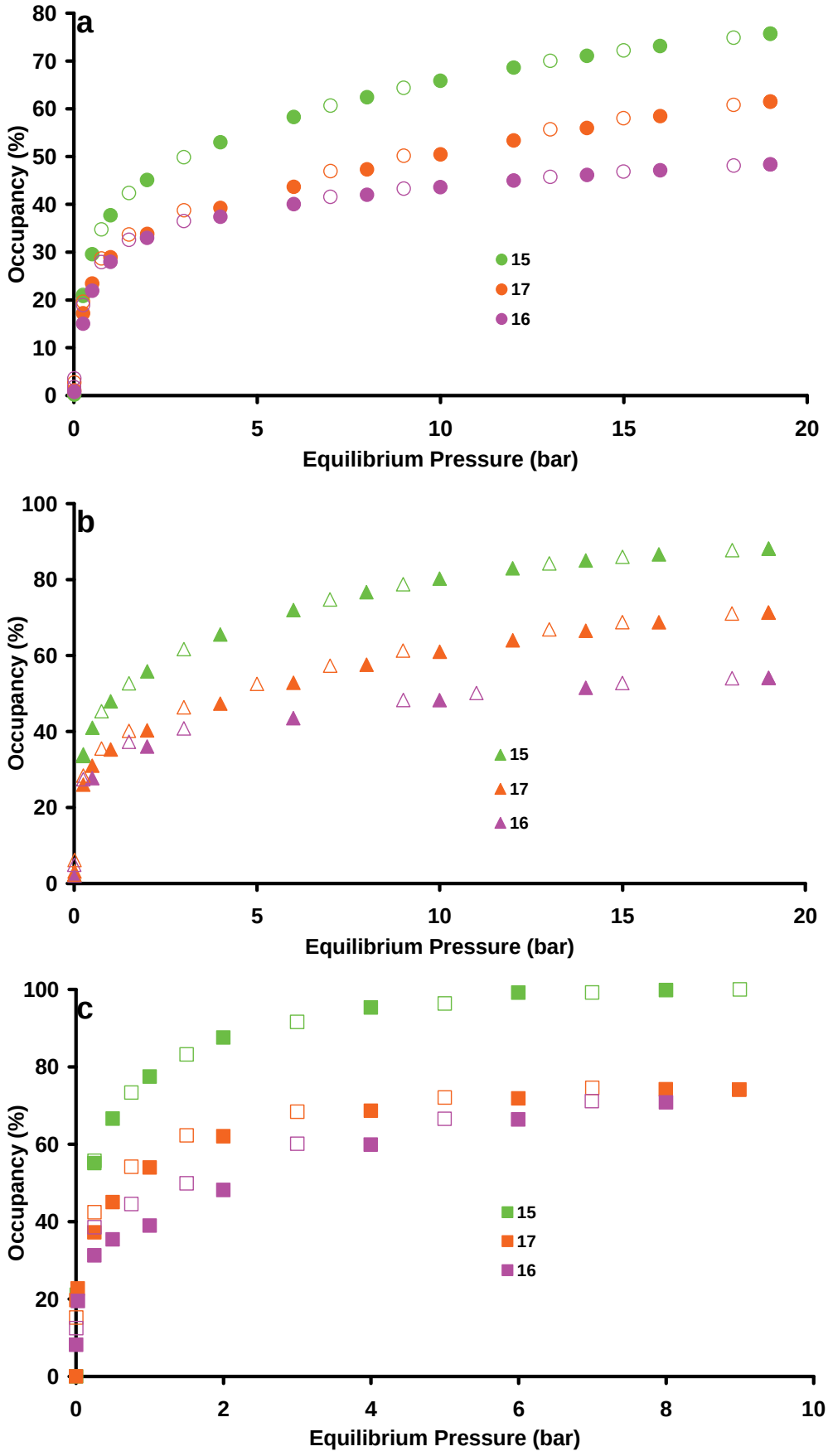

Figure 4.29 CO_2 sorption data for **15-17** at different temperatures: **(a)** 22 ºC (•), **(b)** 0 ºC (▲) and **(c)** -40 ºC (■). Filled symbols indicate absorption and open symbols indicate desorption.

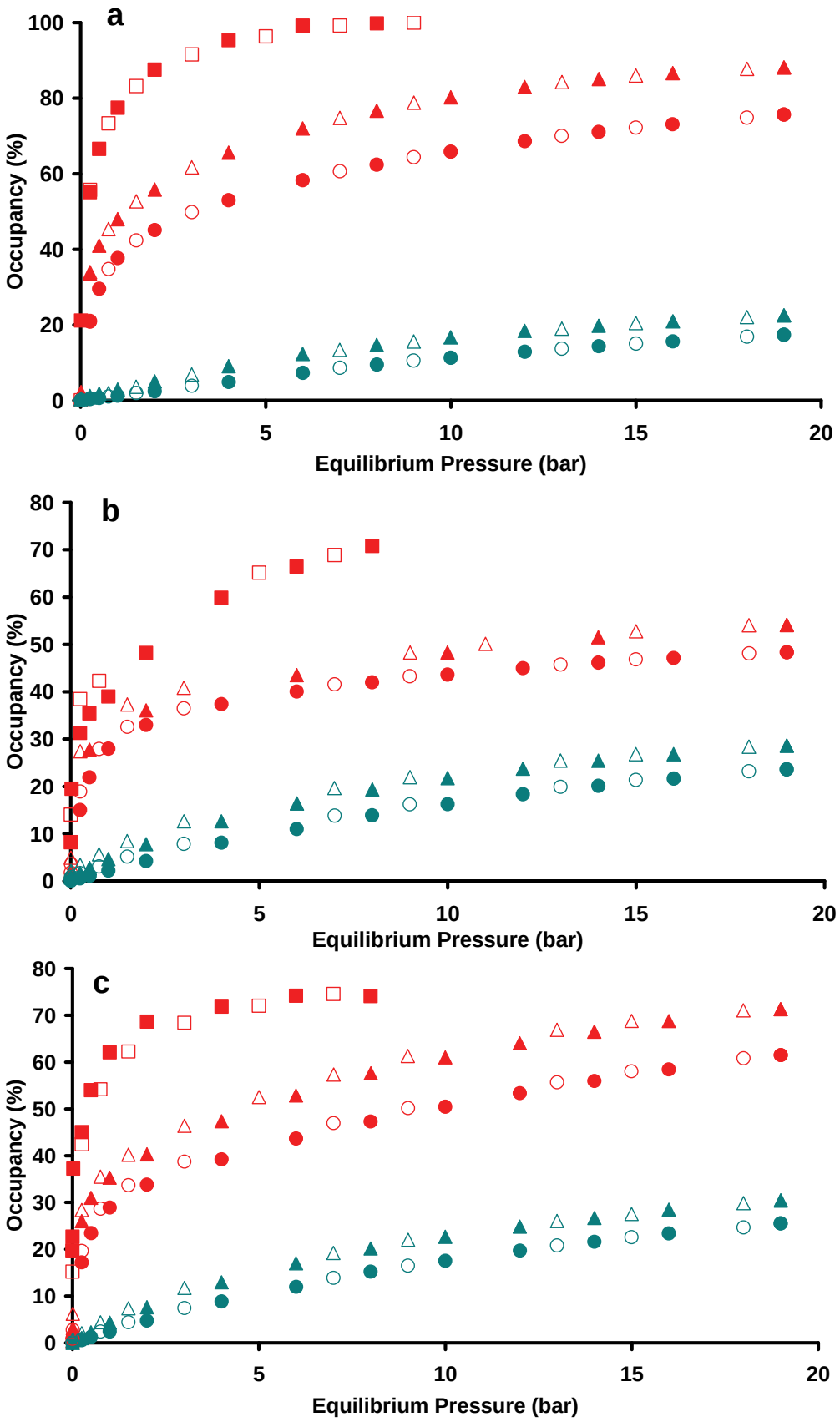

Figure 4.30 Comparison of N_2 (•,▲) and CO_2 (•,▲,■) gas sorption at 22 (•), 0 (▲) and -40 ºC (■) for **(a) 15 (b) 16** and **(c) 17**. Filled symbols indicate absorption and open symbols indicate desorption.

and, when considering the size of guests able to move through the lattice upon desolvation, it can be assumed that the size of the gate is not a significant factor with regard to guest transport and thus, the gas sorption ability of the different materials.

The isotherms shown in Figure 4.30 indicate that sorption of CO_2 is much more favourable than that of N_2. This is attributed in part to the difference in size, with CO_2 capable of more van der Waals surface-interaction with the host. The CO_2 molecule is also more polarisable than N_2, allowing stabilisation from a slight $C(\delta^+)\cdots X^-$ interaction as observed in the single crystal structure of $\mathbf{15_{CO2}}$. It is assumed that the difference in energy of this $C(\delta^+)\cdots X^-$ interaction for the three materials is partly responsible for the difference in CO_2 sorption behaviour (which was also inferred from the single-crystal studies of **15** and **16** under CO_2 pressure), but this postulate needs to be confirmed by computational work.

Since metallocycles are often solvent templated, one anticipates that the methods used in preparation are of some importance to the properties displayed by the product. Growing large quantities of crystalline material from solution can be a very tedious process. Firstly, it is very time-consuming to wait for crystals to grow, especially in the case of the coordination compounds described here, where high dilution of starting materials is required for crystallisation by solvent interdiffusion as a result of the insolubility of the product. Secondly, there is the possibility of obtaining unwanted (*i.e.* inactive) phases. In an attempt to produce these coordination compounds more rapidly, ball-mill grinding under various conditions was investigated. It was hoped that mechanochemistry[36-38] would provide a quick and convenient means of producing these zero-dimensional architectures without the use of large amounts of solvent (as required for high-dilution crystal growth techniques) and that the desired compounds could be produced in larger quantities. Considering that single-crystal X-ray structures of the desired products are already in hand, it would be a simple matter to analyse mechanochemically-produced materials for phase purity using powder diffraction methods. Diffractograms of pulverised products can also be compared to those of the starting materials in order to monitor progress of the reaction (Figure 4.31a). A series of experiments was conducted in which equimolar amounts of CdI_2 and **L** were pulverised for different periods of time together with varying amounts of MeOH and/or CH_2Cl_2. Similar powder patterns with varying degrees of crystallinity

were obtained for most of the grinds, implying that the metallocycle can be templated by either MeOH or CH_2Cl_2. To confirm that the metallocycles could only form if suitable templating molecules were present, a grinding experiment was conducted in the absence of solvent. Powder patterns indicate that the product does not have the same structure as **16**. Indeed, structural details relating to the form obtained by solventless grinding (Figure 4.31d) are not known. Although it is apparent from powder diffraction studies that the ground products include amorphous material (Figure 4.31b and c), the gas sorption ability of one such sample was tested and found to be similar to that of a sample of **16** crystallised from solution (Figure 4.32). It is believed that a systematic study of different grinding conditions might yield reaction conditions that could replace the solvent-diffusion technique for the production of large amounts of sample for gas sorption experiments.

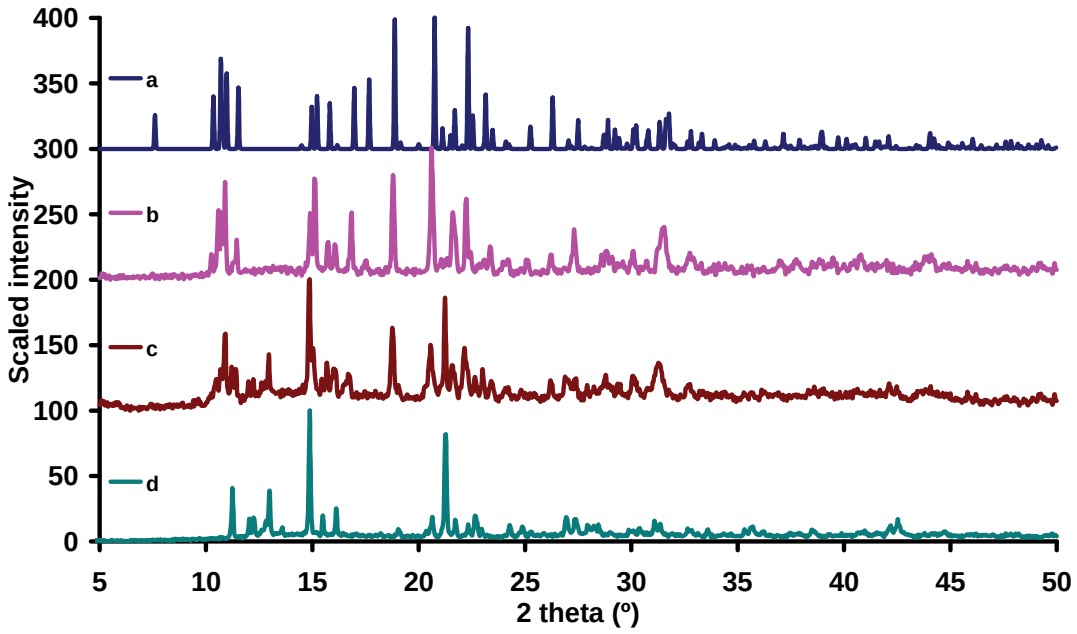

Figure 4.31 **(a)** Simulated powder pattern from $\mathbf{16}_{vac}$ and experimental powder patterns from **(b)** the sample of **16** that was used for gas sorption, **(c)** a sample using 1:1:2.5:2.5 L:M:MeOH:CH_2Cl_2 after ball-mill grinding and **(d)** a sample ground in a ball-mill in the absence of solvent.

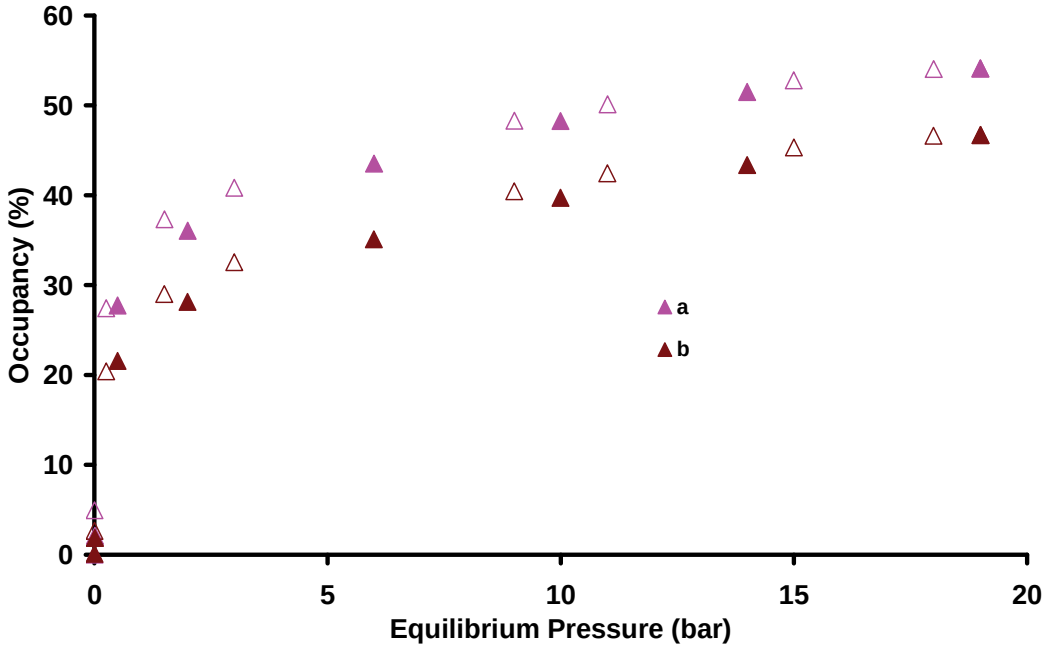

Figure 4.32 Gas sorption isotherms of CO_2 at 0 ºC determined for **(a) 16** grown from solvent and **(b) 16** prepared by ball-mill grinding.

4.2.5 Permeability of single-crystals to bulkier species

To further test the permeability of **15**-**17**, and to confirm that the X3^{i}···X3^{iv} distance (as described in section 4.2.4) is not a significant factor when considering guest sorption by the different halide-substituted metallocycles, larger potential guests were investigated. A crystal of **15** was mounted in the gas cell and exposed to 10 bar of carbonyl sulphide (COS) during intensity data collection at room temperature. The crystal structure of $\mathbf{15_{COS}}$ reveals the presence of one molecule of COS per cavity, with the guest disordered over two positions. Owing to retention of 2/*m* symmetry, the asymmetric guest assumes two opposite orientations in the disordered model (Figure 4.33). Like the guest in the singly-occupied $\mathbf{16_{CO2}}$ structure, the COS molecule is oriented parallel to the Cl···Cl vector, with ∠C–O···Cl^{-} = 174.1º and ∠C–S···Cl^{-} = 171.6º. It is presumed that the void volume is not large enough to accommodate two COS molecules simultaneously. The electron count (determined using SQUEEZE) within the guest-accessible void is 30.8 e^{-} (30 electrons expected for one molecule of COS), suggesting that all the cavities are fully occupied. There is no van der Waals interaction between the guests and hosts, as the cavities are relatively large with a volume of *ca* 143 Å^3 (r_{probe} = 1.4 Å).

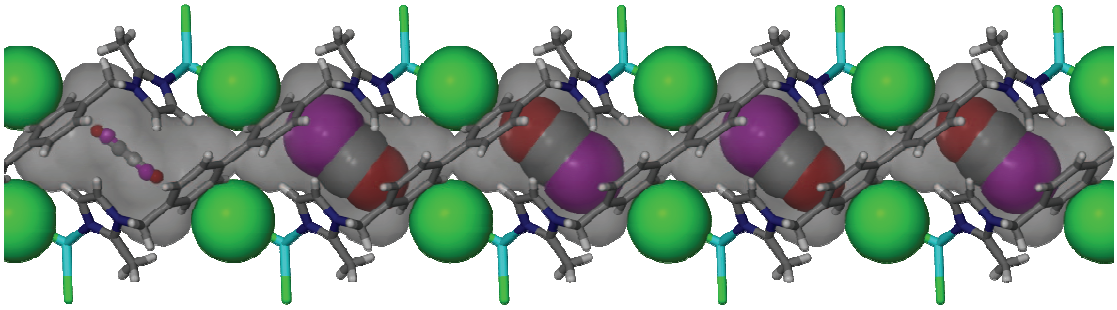

Figure 4.33 Structure of $\mathbf{15_{COS}}$ determined at 22 ºC under a pressure of 10 bar of COS. The void spaces of the cavities are shown as semi-transparent grey surfaces with the host metallocycles shown in capped-stick representation. The chloride anions forming the floor and roof of the mapped cavity are shown in space-filling representation along with the COS molecules, for which only one of the two disordered positions are shown (only the guest of the left-most cavity is shown in ball-and-stick to illustrate the 50/50 disorder). The volume of each guest-accessible void is approximately 143 $Å^3$.

Desolvated crystals of all three compounds **15-17** were immersed in carbon disulfide (CS_2) to establish whether these relatively large molecules could diffuse through the host lattice. CS_2 is bulkier than COS with the van der Waals radius of S = 1.80 and O = 1.52 Å. All three samples were left in carbon disulfide for a number of days and their single-crystal structures were determined at 100 K ($\mathbf{15\text{-}17_{CS2}}$). Surprisingly, almost full occupancy *ca* 76-87% (assuming a potential maximum of one molecule of CS_2 per cavity) was determined using SQUEEZE for all three metallocycles. In all three compounds the CS_2 molecule appear to lie along the length of the cavity with the van der Waals surface of the sulphur atoms slightly intersecting that of the halogens, with $Cl^-\cdots S$ = 3.682(3), $Br^-\cdots S$ = 3.684(3) and $I^-\cdots S$ = 3.667(7) Å (Figure 4.34 and Table 4.5). The vapour sorption isotherms could not be determined as carbon disulfide is not compatible with the Hiden IGA gravimetric system. This is unfortunate because a study of the kinetics of this vapour sorption process for **15-17** would be helpful in establishing whether the sizes of the anions forming the gates to the cavity have an effect on the rate at which guests are absorbed (*i.e.* if significantly different activation energies are at play). Nevertheless, these results indicate that the gating halogens and indeed the structure itself must possess considerable flexibility for a molecule as large as CS_2 to be able to diffuse through the host lattice. Since CS_2 is able to diffuse through all three materials, regardless of the restriction on pore size, it is suggested that the "gate" dimensions are not a significant factor when considering gas sorption ability. However this raises new questions that cannot be addressed by

our initial approach: what is the mechanism of gas transport? Does this process occur by virtue of thermal vibration of the host or is it due to cooperative host:guest interactions?

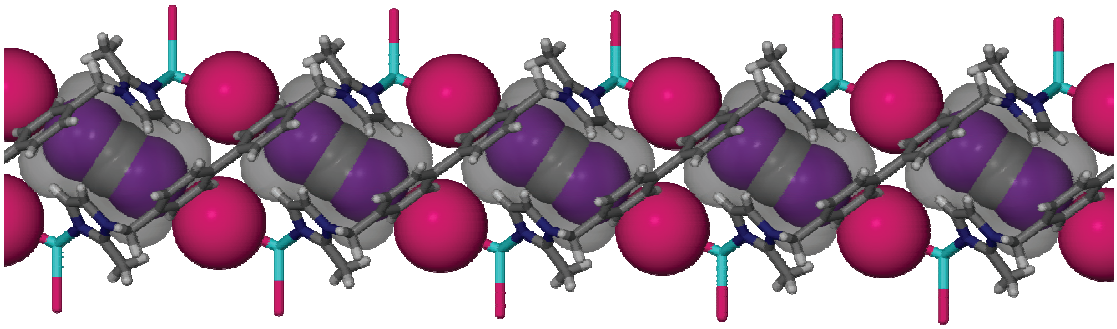

Figure 4.34 $\mathbf{17}_{CS2}$ is shown with the host metallocycles in capped-stick and the guests and iodide anions in van der Waals representation. Guest-accessible volumes are shown as grey surfaces. The structures of $\mathbf{15\text{-}17}_{CS2}$ are all quite similar; even the volumes (*ca* 119.3 for **15**, *ca* 118.9 for **16** and *ca* 120.8 $Å^3$ for **17**) are almost identical for each case.

Table 4.5 Electron counts, occupancies and structural parameters of **15$_{COS}$** and **15-17$_{CS2}$**. Volumes are calculated with r_{probe} = 1.4 Å, the atoms of the COS guest molecule are labeled O17–C18–S19 and the atoms of the guest CS_2 molecule are labeled C17–S18.

	15$_{COS}$	**15$_{CS2}$**	**16$_{CS2}$**	**17$_{CS2}$**
COS pressure (bar)	10	-	-	-
Temperature (°C)	22	-173	-173	-173
Void volume (Å^3)	143	119	119	121
Electron count	30.8	33.1	28.8	33.2
Occupancy (%)	100	87.1	75.8	87.4
Cell length *a* (Å)	17.966(2)	17.790(2)	17.584(3)	17.478(2)
Cell length *b* (Å)	15.608(2)	15.546(2)	16.190(3)	15.809(2)
Cell length *c* (Å)	9.407(1)	9.305(1)	9.419(2)	9.391(1)
Cell angle β (º)	114.26	114.87	113.81	114.46
Cell volume (Å^3)	2405.04	2334.51	2453.26	2362.1
Cd1–N4 (Å)	2.230(3)	2.212(3)	2.226(9)	2.211(4)
Cd1–X3 (Å)	2.414(2)	2.423(1)	2.739(2)	2.554(1)
Cd1–X2 (Å)	2.437(2)	2.449(1)	2.731(2)	2.572(1)
Cd1^{i}···Cd1^{iv} (Å)	8.698(1)	8.454(1)	8.643(2)	8.469(1)
Cd1^{iii}···Cd1^{iv} (Å)	9.250(1)	9.165(1)	8.745(2)	8.877(1)
Cd1^{i}···Cd1^{vi} (Å)	15.580(2)	15.236(2)	15.823(3)	15.525(2)
Cd1^{ii}···Cd1^{iii} (Å)	16.507(2)	16.422(2)	15.990(3)	16.195(2)
Cd1^{ii}···Cd1^{v} (Å)	25.227(3)	25.071(2)	24.745(4)	24.943(3)
X3^{i}···X3^{iv} (Å)	5.728(5)	5.561(4)	5.358(3)	5.331(2)
X3^{i}···X3^{vi} (Å)	10.791(4)	10.430(3)	10.396(3)	10.449(2)
X3^{iii}···X3^{iv} (Å)	11.232(5)	11.236(4)	11.259(3)	11.138(2)
X3···O17 (Å)	3.81(1)	-	-	-
∠X3···O17–C18 (º)	171.6	-	-	-
∠Cd1–X3···O17 (º)	173.7	-	-	-
X3···S18 (Å)	-	3.682(3)	3.667(7)	3.684(3)
∠X3···S18–C17 (º)	-	171.0	180.0	176.1
∠Cd1–X3···S18 (º)	-	173.9	170.2	173.2

Symmetry codes: (i) –x, y, 2-z; (ii) x, y, 1+z; (iii) –x, y, 3-z; (iv) x, y, 2+z; (v) –x, y, 4-z; (vi) x, y, 3+z.

4.2.6 The mechanism of guest movement through the host – molecular mechanics and statistical mechanics calculations[§]

In order to better understand the gas sorption process in the context of the host:guest structural results, it was decided to investigate the possible mechanism by which gas transport occurs through the lattice. This investigation includes modelling studies as well as physico-chemical measurements of kinetic and thermodynamic parameters.

In considering the host thermal displacement parameters obtained for the atoms of $\mathbf{15_{vac}}$ versus those of $\mathbf{15_{2,C2H2}}$ and $\mathbf{15_{16,C2H2}}$ (Figure 4.35), it appears that there is a decrease in atomic motion as pressure increases. This supports the notion that guest molecules diffuse through the host as a result of a rapid and spontaneous "shivering" (regardless of the presence or absence of guests) by the host metallocycles, whereby neighbouring voids may become interconnected momentarily, and that guest molecules seize this opportunity to "jump" between cavities. This is not a novel idea – molecular mechanics simulations for a CO_2 guest molecule diffusing through a similar host system mentioned in section 4.1 had already paved the way for the formulation of this concept.[39] From the thermal ellipsoid plots it becomes apparent that the 2-methylimidazole moieties swivel around the N4–N7 vector, as implied by the elongated thermal ellipsoids of atoms C5, C6 and C9. These ellipsoids indicate that movement of these atoms could facilitate the fleeting union of two adjacent voids into a single cavity. Figure 4.35a illustrates how the displacement of these atoms is more pronounced in the absence of guests and, as the occupancy of acetylene guest molecules within the cavities increases from vacuum to the 2 bar (*ca* 50% occupancy) and 16 bar (*ca* 100% occupancy) structures, the host most likely becomes more rigid and less guest movement takes place. This postulate corresponds with the decrease in observed thermal movement (Figure 4.35b and c).

[§] Experiments and calculations mentioned in 4.2.6 were conducted by various co-workers and the relevant references should be consulted for more detail.

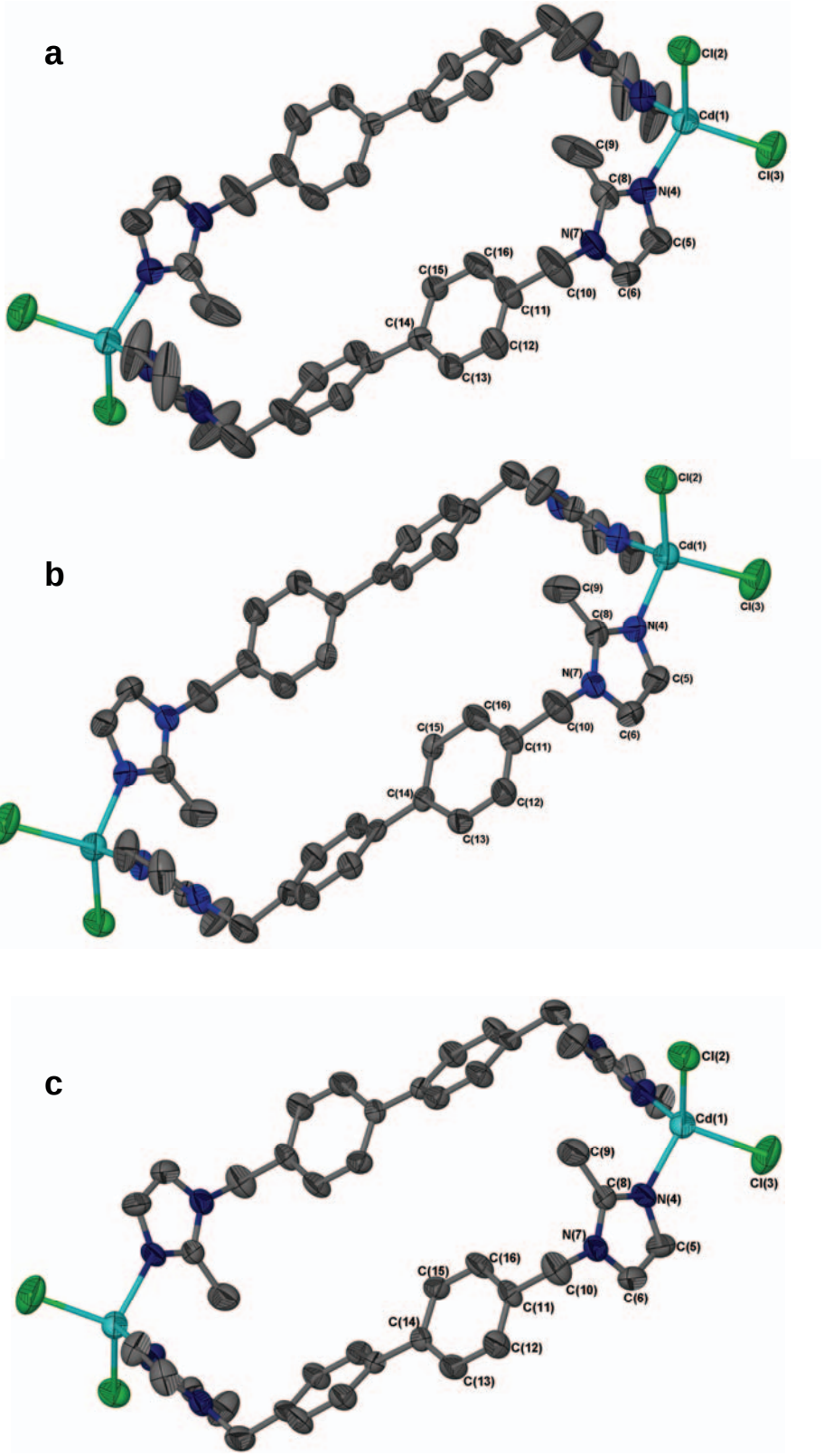

Figure 4.35 Three 50% probability thermal ellipsoid plots are shown viewed along (110), these were determined from single-crystal diffraction data and the numbering indicates the crystallographic asymmetric unit of the metallocycle. **(a)** The vacuum structure of **15**, **(b)** the 2 bar C_2H_2 structure of **15** and **(c)** the 16 bar C_2H_2 structure of **15**, where C_2H_2 guest molecules have been omitted.

From the isosteric heats of sorption for CO_2 (ΔH_{iso}, Figure 4.36) reported by Marais,[40] the value determined for ΔH_{iso} at the lowest pressure used (62 mbar) is -30 kJ.mol^{-1}. While this is relatively low in magnitude, binding of CO_2 in the empty pockets is still favourable.

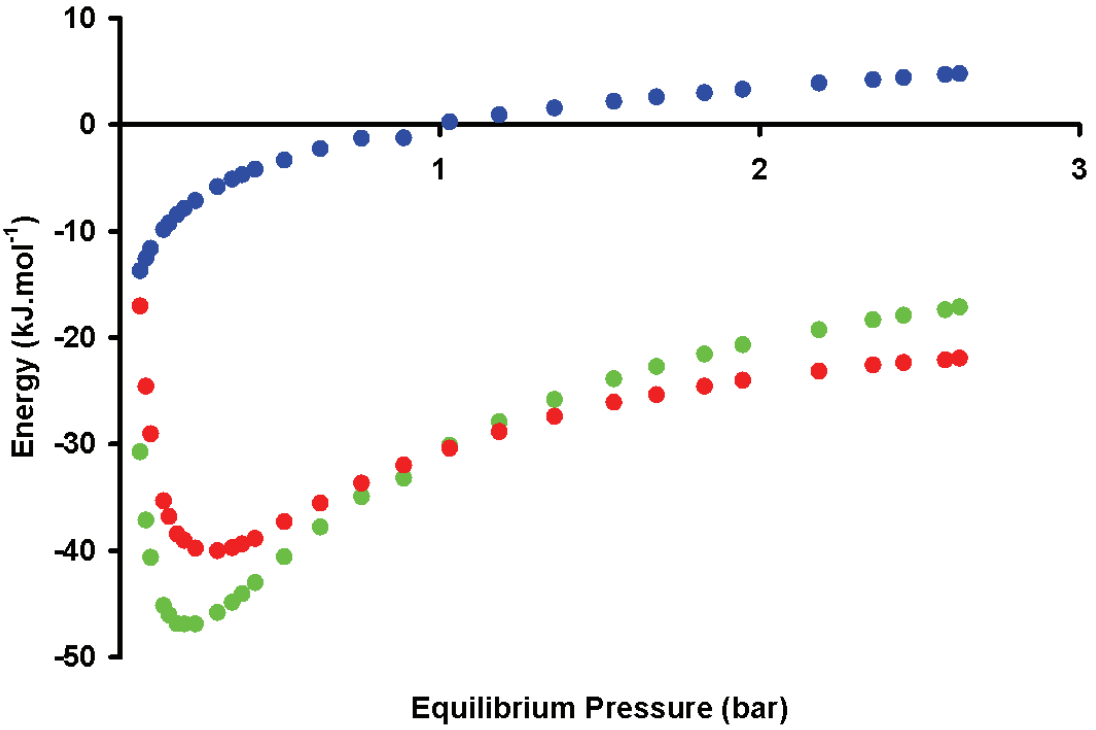

Figure 4.36 Thermodynamic parameters of CO_2 sorption for the metallocycle **15**: $\Delta G°_{ad}$ (●), $T\Delta S°_{ad}$ (●) and $\Delta H°_{ad}$ (●).[40]

The rate of CO_2 sorption by **15** at different temperatures was also investigated by Marais in order to corroborate the proposed reaction mechanism, and to determine values for the kinetic parameters.[40] This experiment involved recording isothermal CO_2 sorption at various temperatures and a fixed pressure by monitoring the extent of the reaction (α) with time (Figure 4.37). These data were then analysed using a number of known functions $f(\alpha) = kt$, and selecting the relationship that best fits the data to a straight line as being representative of the process. The most appropriate kinetic model for describing the sorption data was determined to be the deceleratory (v_{max} at $t = 0$) α-time curve based on three dimensional diffusion (D3).[41] Here it needs to be stated that solid-state reactions such as this can occur in multiple steps, which would imply a possible change in kinetic parameters with loading, but kinetic models that are currently used are simplified by assuming a one-step reaction.[42] It is stated in

the literature that better-formulated kinetic models are necessary for the more accurate description of solid-state reactions.[42] However, this shortcoming notwithstanding, this result is in excellent agreement with the gas transport mechanism proposed above since diffusion is generally a non-activated (spontaneous) process. These experiments were conducted at a constant pressure of 1400 mbar and at temperatures ranging from -43 to 50 °C.

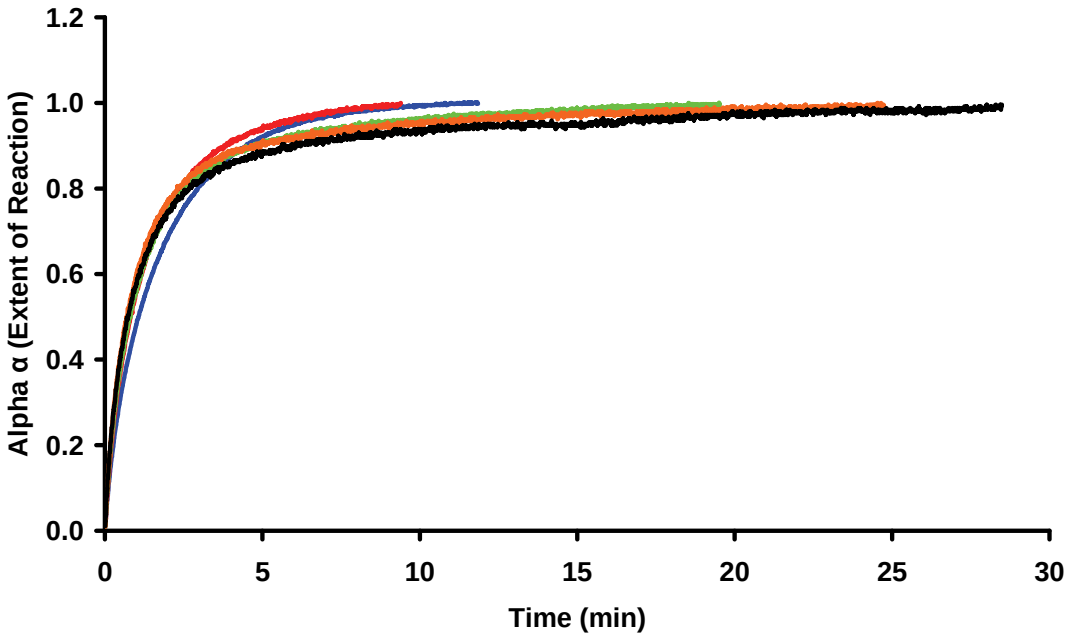

Figure 4.37 Alpha-time plots of **15** undergoing sorption reactions with CO_2 at various temperatures: -43 °C (■); -15 °C (■); 0 °C (■); 24 °C (■) and 50 °C (■). There appears to only be a very slight temperature dependence on the rate of sorption, but this is practically negligible.[40]

For each of the α-time plots recorded at a specific constant temperature, a value of the rate coefficient k can be determined using the empirically selected rate law (kinetic model). An Arrhenius plot (*i.e.* ln k values against T^{-1}, Figure 4.38) can be used to determine the activation energy (E_a) for the gas sorption process. The almost negligible gradient (which corresponds to E_a = -9.27 J.mol^{-1}) of the curve shows that the activation energy is approximately zero (for practical purposes) for the uptake of CO_2 molecules at 1400 mbar. This activation energy is sufficiently low to imply that sorption is a non-activated process in the temperature range investigated, and this observation is consistent with the diffusion model that has been postulated. Once again, it should be noted that E_a and A are presumed to remain constant during the entire course of the reaction – however, it has been shown that such assumptions do

not always hold for solid-state reactions.[42] Although there has been some controversy over the validity of applying the Arrhenius equation to heterogeneous reactions,[43] alternative empirical functions that have been proposed do not offer any significant advantages. Galwey and Brown have justified the use of the Arrhenius equation for heterogeneous reactions and have shown how the rate coefficients for Arrhenius plots can be directly extracted from alpha-time plots without knowledge of the specific kinetic model. This, however, is not applicable in the case of the diffusion models.[44]

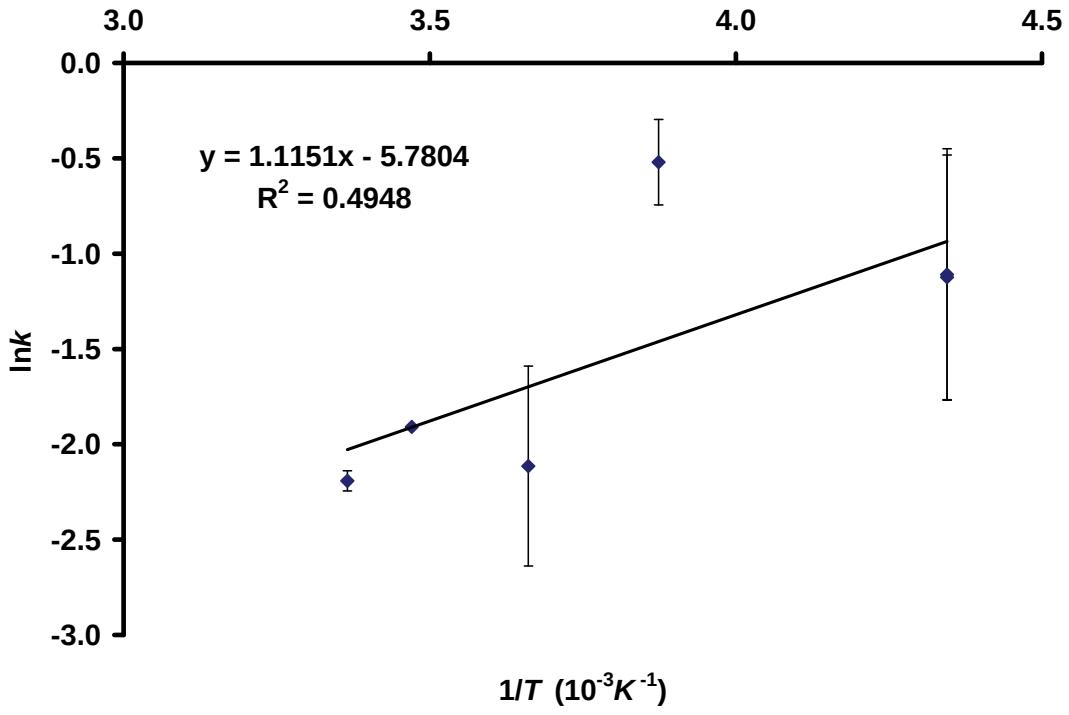

Figure 4.38 Arrhenius-plot of **15**, implying that the sorption of carbon dioxide is a non-activated process.[40]

Better methods of determining thermodynamic and kinetic parameters and kinetic models for solid-gas sorption reactions are still under development and the results presented here should only be considered as preliminary findings. However, in conjunction with other methods used as part of this study (*i.e.* single-crystal diffraction studies, gas sorption and computational methods), these results can still provide useful information about possible mechanisms.

As mentioned in section 4.2.3, when CO_2 or C_2H_2 is sorbed by **15**, a given cavity can assume only one of three possible occupancy states at any time: it can be empty, occupied by a single guest or doubly occupied. It seems self-evident that the

probability for a given cavity to assume any one these states must be governed by the equilibrium pressure. It is of interest to investigate whether it is possible to deconvolute the sorption isotherm into the probabilities for the three states as a function of pressure. To this end, statistical mechanical sorption models of **15** with both CO_2 and C_2H_2 were developed by Müller-Nedebock.[45**]

The three occupancy states can be simplified using three potential energy wells (Figure 4.39). The steeper the sides of the potential well, the greater the rigidity of the cavity. As occupancy of the cavity increases, the energy minimum of the cavity rises with a correspondingly larger energetic penalty for deformation of the host framework. The Cl···Cl distance (as determined from the single-crystal structures, see $Cl3^{i}\cdots Cl3^{vi}$ in Table 4.2 and Table 4.3) was selected as an indication of cavity deformation along its major axis (plotted on the abscissa).

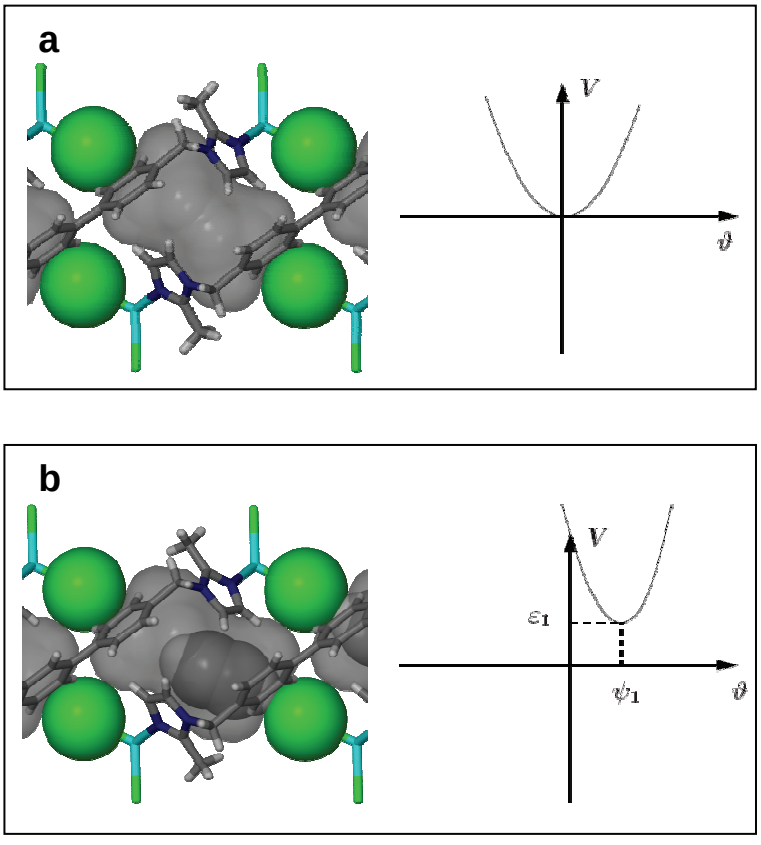

** Statistical mechanics calculations were performed by Prof. K. Müller-Nedebock of the Department of Physics at the University of Stellenbosch and he should be consulted for more information.

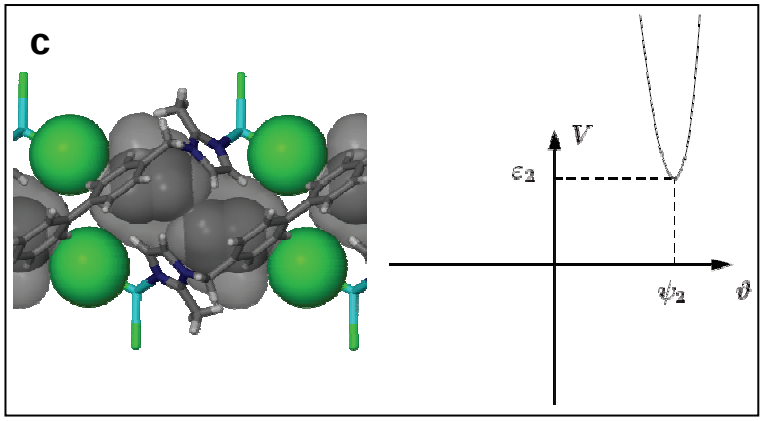

Figure 4.39 The three possible occupancy states of a given cavity. **(a)** When a cavity is empty it constitutes a minimum energy state for the host and deformation can occur more readily for this state than for any other. **(b)** With one acetylene molecule in the cavity, the minimum energy of the cavity is slightly higher and the cavity is less likely to deform than the empty cavity (*i.e.* an energetic penalty has been incurred due to deformation of the cavity, and the rigidity of the metallocycle increases). **(c)** A doubly occupied cavity represents the highest energy state of the three possibilities and deformation results in a large energetic penalty, as indicated by the very steep curve.

Statistical mechanics calculations were then carried out using computationally derived host:guest interaction energies and the cavity deformation parameter, and by making two basic assumptions: (i) that the crystal is one-dimensional and (ii) that elastic coupling occurs between neighbouring voids. Elastic coupling is the deformation that occurs when the conformation of a void is influenced by the amount of distortion in neighbouring voids.

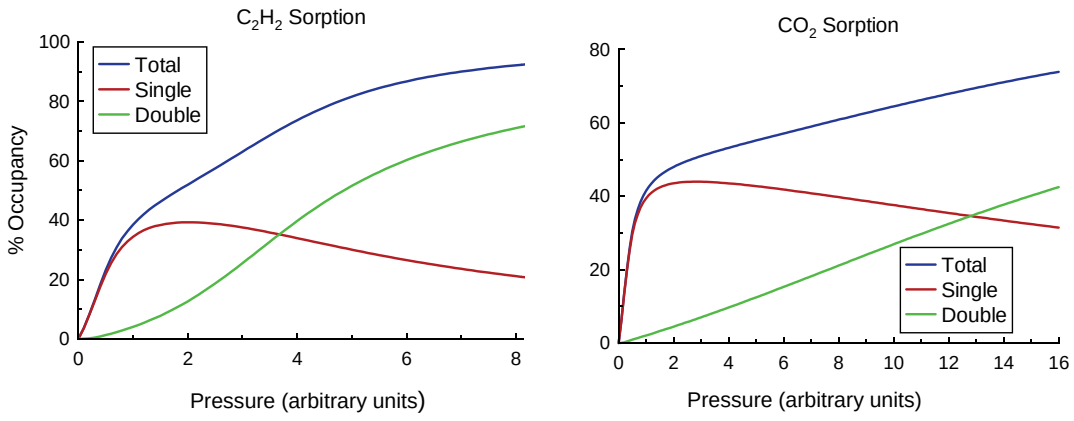

Figure 4.40 Statistical mechanics calculations predicting the probabilities for occupancy as a function of pressure for C_2H_2 and CO_2 (actual gas sorption data were not used for these calculations).

Percentage probability plots for the various states of a given cavity (as a function of pressure in arbitrary units) for CO_2 and C_2H_2 are given in Figure 4.40. The red curves show the probability for single occupancy, green the probability for double occupancy and the blue curve represents the sum of the two occupancy states (at any pressure, zero-occupancy probability can be inferred as total occupancy subtracted from 100). In order to compare the statistical mechanical results to the experimentally determined sorption isotherms, it is only necessary to scale the horizontal axis of the former. Figure 4.41 shows the excellent agreement between the experimental gas sorption data (black dots) and the statistically modelled values.

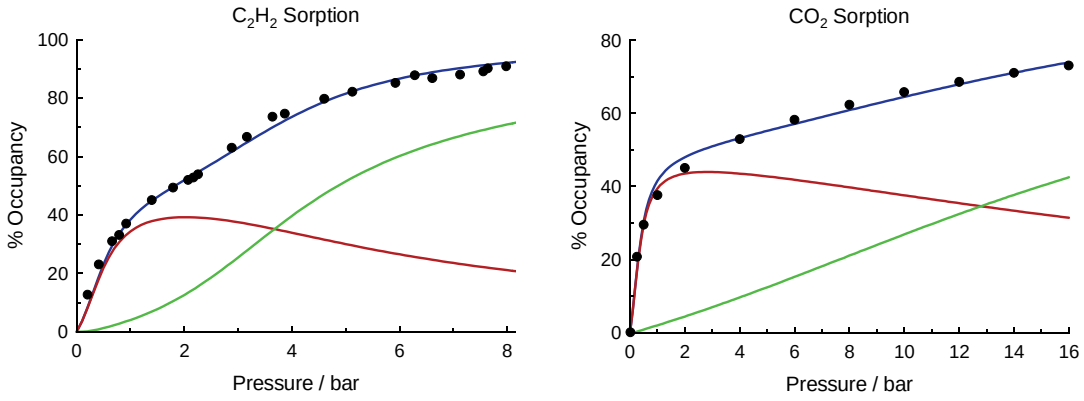

Figure 4.41 The theoretical functions shown in Figure 4.40 appear to agree well with the experimental data (black circles) after suitable scaling of the former along the abscissa.

As discussed above, the host lattice undergoes significant distortion to accommodate two molecules of C_2H_2, whereas comparatively little distortion accompanies CO_2 uptake. In considering the green curves of Figure 4.40, it appears that doubly occupied cavities are far less probable for C_2H_2 at low pressure (*i.e.* below 50% overall occupancy) than for CO_2. Presumably this is because, when C_2H_2 is sorbed, the lattice first has to undergo a guest-induced deformation around 50% average occupancy before double-occupancy becomes favourable. Since no significant host deformation is necessary for CO_2 sorption to take place, the probability of a doubly occupied cavity remains directly proportional to the equilibrium pressure throughout the sorption process. The assumption of elastic coupling between voids also produces an inflection in the calculated isotherm for C_2H_2 at *ca* 2.7 bar, which coincides almost exactly with the inflection observed for the experimental data.

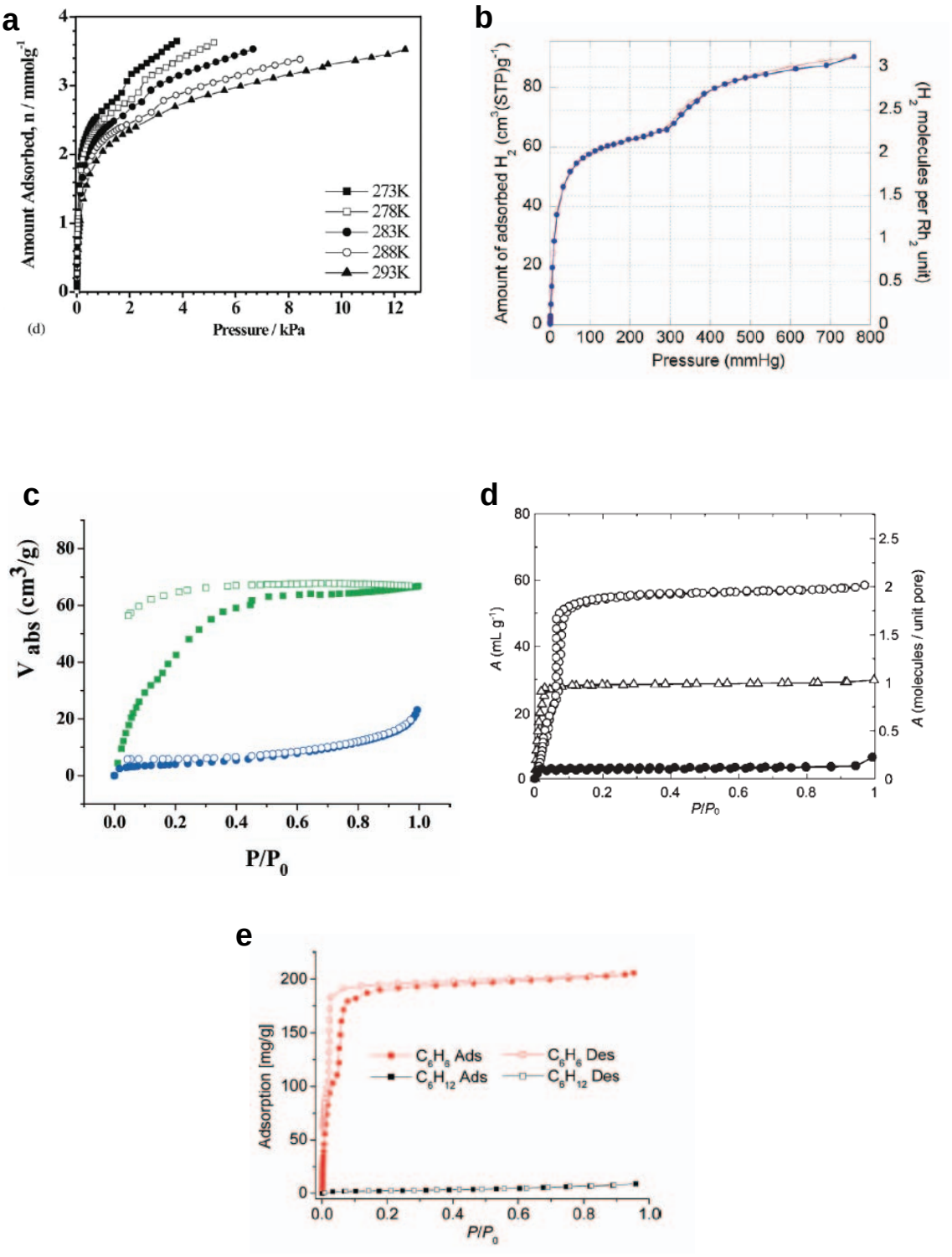

Figure 4.42 **(a)** A sorption isotherm for methanol shows an inflection at 66% loading (*i.e.* 2 molecules) (A. J. Fletcher, K. M, Thomas and M. J. Rosseinsky).[46] **(b)** When hydrogen is sorbed an inflection is observed when a third molecule is sorbed per Rh_2 unit (S. Takamizawa and E.-I. Nakata).[47] **(c)** Hydrogen is sorbed, but no details of the structure are given (B. Chen *et al.*).[48] **(d)** A vapour sorption isotherm, where 2 methanol molecules are sorbed and a discontinuity is seen at 50% loading (S. Horike, D. Tanaka, K. Nakagawa and S. Kitagawa).[49] **(e)** Step in both the adsorption and

desorption isotherms are observed near the uptake level of two molecules of benzene per cage (J.-P. Zhang and X.-M. Chen).[50]

The literature was consulted in an attempt to locate more examples where flexible porous systems produced isotherms with inflection points. Several such instances were encountered and these are shown in Figure 4.42. Only two of these reports offer an explanation for the inflection: (i) in accounting for Figure 4.42a, the authors state that "…when the third methanol guest per formula unit is sorbed, the structure is forced to readjust to accommodate it, producing both the isotherm step and the slow kinetics at this point"; (ii) Takamizawa and Nakata provide the following statement about their isotherm (Figure 4.42b), "…two-step adsorption was observed at around 300 mmHg with an adsorption of 66 $cm.g^{-1}$, indicating that the two H_2 molecules per Rh_2 unit or channel period are at the first of the stable adsorbed states…"

Using only parameters obtained from the single-crystal gas study (*i.e.* lattice deformation and host:guest intermolecular energies calculated from atomic coordinates), it was possible to model a deconvoluted gas sorption isotherm of occupancy as a function of pressure by means of statistical mechanics. All the techniques mentioned have provided a large amount of information on the gas transport mechanisms and adsorbent-adsorbate and adsorbate-adsorbate interactions at play during these processes. It can be stated with some confidence that guest transport is a non-activated process for the smaller gas species (CO_2 and C_2H_2). It would, however, be of considerable interest to also employ molecular mechanics simulations for the CO_2 and C_2H_2 diffusion in order to visualise the process of filling an initially empty cavity first with one guest molecule, and then with a second. It would then be of further interest to compare this process to a simulation involving diffusion of a larger guest such as CS_2, which can only take on a single-occupancy state.

4.3 CONCLUSION

This chapter describes an extension of our approach to constructing potentially porous materials using zero-dimensional (*i.e.* discrete) dinuclear metal complexes. These entities are self-assembled from metal ions and ditopic imidazole-derived ligands with rigid spacers. The self-assembly of five analogous molecular hexagons from different

metal ions and the novel ligand 4,4′-bis(2-methylimidazol-1-ylmethyl)biphenyl (**L**) has been described. Rearrangements of the coordination compounds $\mathbf{13_{MeOH}}$ and $\mathbf{14_{MeOH}}$ (metallocycles constructed from $ZnCl_2$ and $CoCl_2$) upon solvent loss have been described owing to the occurrence of single-crystal to single-crystal transformations. Furthermore, the reaction of **L** with cadmium and different halide anions leads to the successful synthesis of three discrete cadmium metallocycles (with Cl, Br and I). These metallocycles include solvent upon formation, and subsequent removal of guest species occurs without rearrangement of the host lattice, thereby affording three novel porous compounds **15-17**. An acetylene gas sorption isotherm was determined for **15** using a locally-developed volumetric gas sorption instrument. Gas sorption isotherms of CO_2 and N_2 at variable temperatures were determined for **15-17** using a commercial gravimetric gas sorption instrument. These studies were undertaken in order to determine the influence of the electrostatic profile of the cavity on guest sorption ability.

As part of this study, a miniature gas cell was developed to facilitate single-crystal intensity data collection on a conventional diffractometer while exposing a crystal to a constant and controlled gas pressure. The cell is small enough to allow use of a routine data collection strategy such that either a sphere or hemisphere can be collected (as deemed necessary). With the aid of this simple device, an unprecedented level of detail has been obtained with regard to structural changes that accompany the uptake of gas by a host at various systematically-controlled pressures. Specifically, carbon dioxide and acetylene, two gases with similar dimensions but different electrostatic surfaces, were investigated. Although their sorption behaviours differ only slightly, the high level of structural detail obtained during this study allows rationalisation of these differences in terms of host:guest interactions, as well as packing considerations (*i.e.* the step-wise filling of a well-defined void volume to reach a maximum occupancy of two guest molecules per cavity). Furthermore, we have shown that electron counts (using difference electron density maps) within the cavities provide a reasonable, albeit tedious, alternative to conventional sorption data for determining occupancies, thus bypassing the associated problems of bulk phase purity. Indeed, it is remarkable that as little material as one single crystal can be used for this purpose. Future routine application of our method in conventional X-ray diffraction laboratories promises to yield significant advances in the field of gas

sorption research by providing an improved understanding of processes that occur at the molecular level.

It is of further interest that the uptake of gas and diffusion of solvent occurs despite the apparent lack of channels linking the voids: a plausible explanation for this involves the spontaneous formation of short-lived channels as a result of dynamic motion of the framework components, as inferred from the atomic displacement parameters. These indicate that the X^- ions guarding the gates between cavities and the imidazole moieties undergo the largest displacement, suggesting a continuous gating process that allows gas molecules to pass through. This proposed mechanism of gas transport is supported by kinetic studies of CO_2 sorption by **15** that suggest a non-activated diffusion model at an equilibrium pressure of 1.4 bar. Complementary molecular mechanics simulations of diffusion of CO_2, C_2H_2, COS and CS_2 may also prove to be useful for determining if the guest transport mechanism is identical in all of these cases (where a 1:2 H:G ratio is observed for CO_2 and C_2H_2 and a 1:1 H:G ratio for COS and CS_2). In addition, CS_2 (which is far larger than CO_2) appears to diffuse through the lattice with little regard for the constriction of the pore size (*i.e.* as inferred from the $X^-\cdots X^-$ distance). Guest transport occurs even though the distance between the halide anions (using static van der Waals surfaces) forming the gate between successive cavities decreases from Cl to Br to I (from **15** to **17** to **16**). From these results, it is apparent that the pore leading into the cavity does not play a significant role in the sorption capacity of the material (when measured at a specific overpressure), since even large molecules are observed to diffuse through the lattice with great ease. On the other hand, this highlights the importance of the stabilisation gained from the host:guest intermolecular interactions, which seem to be the most important factor governing the behaviour of this series of metallocycles.

Ongoing studies are still aimed at tailoring these metallocyclic compounds and, towards this goal, the synthesis of a discrete coordination compound from **L** and cadmium fluoride is currently under way. The rationale for this study is that fluorine possesses unique electronic character as the most electronegative element. Furthermore, since fluoride is relatively small compared to the other halides, formation of an isostructural lattice might result in merging of the cavities to yield an open framework. The effect that a larger anionic ligand will have on the cavity

should also be investigated – for example, using dicarboxylates such as malonic acid or succinic acid. Other "crystal engineering" alterations can also be made to the host compound: *i.e.* using different rigid spacers in the ligands that will hopefully also produce analogous cyclic coordination complexes.

Further computational studies should also be conducted to clarify the energetic differences between the host:guest interactions in the different halides. It is known that cooperative host:guest interactions play an important role in sorption processes involving these seemingly nonporous porous systems. Compound **15** was observed to absorb the most CO_2 and N_2, followed by compounds **17** and **16**. To investigate these findings further, comparative isosteric heat of adsorption and kinetic experiments should also be conducted for **15**-**17**. Such a study could provide valuable information about the influence of the anion on the rate of reaction (if any), and whether the increased size and decreased electronegativity of the halide has any effect on the mechanism of guest transport through the host framework.

4.4 GENERAL PROCEDURES AND INSTRUMENTS

4.4.1 Synthesis and Characterisation

4.4.1.1 4,4′-bis(2-methylimidazol-1-ylmethyl)biphenyl (L)

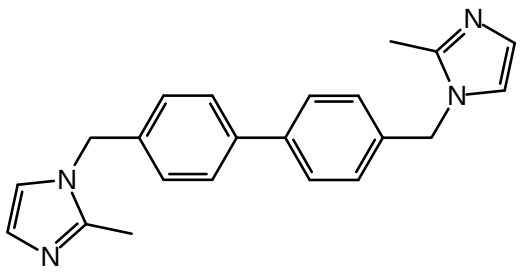

4,4′-Bis(chloromethyl)-1,1′-biphenyl (7 mmol, 1.76 g), 2-methylimidazole (17.5 mmol, 1.44 g) and potassium carbonate (45.5 mmol, 6.30 g) were suspended in 60 ml acetonitrile. The reaction was then stirred under reflux for 10-15 hours. The reaction mixture was orange, forming a beige precipitate. The precipitate was removed by filtration and the solvent was then removed under vacuum to produce orange oil. The crude product was taken up in chloroform and washed with water, dried ($MgSO_4$), filtered and the solvent removed under reduced pressure. The orange oil that results solidifies with addition of diethyl-ether. The product can be precipitated by dissolution in chloroform and drop wise addition of the chloroform

solution to pentane. Further purification was effected by subliming the off-white material at 260-300 °C (2-3 mm Hg).

Yield: 55.5%; M.p. 169-171°C; **δ_H ($CDCl_3$, 400 MHz)** 2.355 (3H, s), 5.082 (2H, s), 6.864 (1H, d, ^3J = 1.32), 6.967 (1H, d, ^3J = 1.20), 7.116 (2H, d, ^3J = 8.33), 7.520 (2H, d, ^3J = 8.30, H-3); **δ_C ($CDCl_3$, 100 MHz)** 13.12, 49.37, 119.85, 127.11, 127.45, 127.52, 135.67, 140.05, 144.90; MS (EI^+) m/z 342 ($M^{+\cdot}$), m/z 261 (100%, $M^{+\cdot}$ – 2 – methylimidazole), m/z 180 ($[CH_2\text{-}C_6H_4C_6H_4\text{-}CH_2]^{+\cdot}$).

4.4.1.2 $[Co_2L_2Cl_4]\cdot 2MeOH$ (13_{MeOH})

0.04 mmol **L** (13.70 mg) were dissolved in 2 ml chloroform and layered with 0.04 mmol $CoCl_2\cdot 6H_2O$ (9.52 mg) dissolved in 2 ml methanol. After three days blue needle-shaped crystals had grown and were suitable for single-crystal diffraction studies.

4.4.1.3 $[Zn_2L_2Cl_4]\cdot 2MeOH$ (14_{MeOH})

0.03 mmol **L** (10.27 mg) were dissolved in 2 ml chloroform and layered with 0.03 mmol $ZnCl_2$ (4.09 mg) in 2 ml methanol. After a week, colourless rods were afforded and the structure elucidated by single-crystal diffraction analysis.

4.4.1.4 $[Cd_2L_2Cl_4]\cdot 2MeOH$ (15_{MeOH})

0.03 mmol **L** (10.27 mg) were dissolved in 2 ml chloroform and layered with 0.03 mmol $CdCl_2\cdot 2.5H_2O$ (4.09 mg) in 2 ml methanol. After 3 days, colourless rod-shaped crystals had deposited and the structure could be determined by X-ray diffraction analysis.

4.4.1.5 $[Cd_2L_2I_4]\cdot CH_2Cl_2$ (16_{CH2Cl2})

0.02 mmol **L** (6.85 mg) were dissolved in 3 ml dichloromethane and layered with 0.02 mmol CdI_2 (7.32 mg) dissolved in 3 ml acetonitrile. After 10 days colourless plates had grown and these were suitable for single-crystal diffraction studies.

4.4.1.6 $[Cd_2L_2I_4]\cdot CH_3Cl$ ($\mathbf{16_{CHCl3}}$)

0.02 mmol **L** (6.85 mg) were dissolved in 3 ml chloroform and layered with 0.02 mmol CdI_2 (7.32 mg) dissolved in 3 ml methanol. After a month, colourless plates were afforded and the structure was elucidated by single-crystal diffraction.

4.4.1.7 $[Cd_2L_2Br_4]\cdot 2MeOH$ ($\mathbf{17_{MeOH}}$)

0.02 mmol **L** (6.85 mg) were dissolved in 3 ml chloroform and layered with a 4 ml buffer layer followed by 0.02 mmol $CdBr_2\cdot 4H_2O$ (6.9 mg) dissolved in 3 ml methanol. After 4 days, colourless plates were afforded and the structure was elucidated by single-crystal diffraction.

4.4.2 Gas sorption experiments

4.4.2.1 Volumetric gas sorption

The method is described in section 2.6. A sample of $\mathbf{15_{MeOH}}$ was crushed and exposed to vacuum for 24 hours in order to remove all traces of methanol solvent. A 1.5060 g (1.432 mmol) sample of pure **15** thus obtained was placed in the sample chamber (V_b = 7.87 cm^3). The volume of the gas reservoir was determined to be V_a = 8.08 cm^3 while the free volume in the sample chamber was $V_b - V_{sample}$ = 6.84 cm^3. Sorption isotherms were determined using a low-range pressure transmitter (0-8 bar) for sample chamber A and an even lower range pressure sensor for sample chamber B (0-4 bar). After completion of these experiments, the pressure transmitters were changed to handle higher pressures, with a 0-16 bar transmitter on chamber A and a 0-8 bar transmitter on chamber B. For this second set of measurements, a 1.4650 g (1.393 mmol) sample of **15** was placed in the sample chamber (V_b = 7.78 cm^3), with the volume of the gas reservoir, V_a = 7.88 cm^3, and the free volume in the sample chamber, $V_b - V_{sample}$ = 6.77 cm^3. Both sets of experiments were conducted at a temperature of 22 ºC.

4.4.2.2 Gravimetric gas sorption

In order to remove all traces of solvent, samples of $\mathbf{15_{MeOH}}$ and $\mathbf{17_{MeOH}}$ were evacuated for 24 hours at room temperature, while $\mathbf{16_{CH2Cl2}}$ was heated to 130 ºC and evacuated for 30 hours. Samples of 87, 66 and 31 mg metallocycle were used for

15-17, respectively. Sorption experiments were conducted at 22 and 0 ºC using a water-bath thermostat and at -40 ºC using a liquid nitrogen controlled thermostat.

4.4.3 Computational methods[††]

The geometry of **13** was optimised at the gradient-corrected DFT level using the three parameter fit of the exchange-correlation potential suggested by Becke[51] in conjunction with the LYP[52] exchange potential (B3LYP).[53] The LANLDZ basis set[54,55] was employed in the geometry optimisation. The nature of the stationary point was examined by calculating the Hessian matrix at this level: the structure is an energy minimum on the potential energy surface. The optimised structure was placed in the same relative conformations as the experimental crystal structures. Single point calculations were performed using B3LYP. The calculations were performed with a parallel version of the program package Gaussian 03.[56]

[††] Calculations were conducted by Dr C. Esterhuysen of the Department of Chemistry and Polymer Science at the University of Stellenbosch and further information is available from her.

REFERENCES

1 J. L. Atwood, L. J. Barbour, A. Jerga, *Science* **2002**, *296*, 2367-2369.

2 D. M. Rudkevich, *Eur. J. Org. Chem.* **2007**, 3255-3270.

3 O. M. Yaghi, M. O'Keeffe, N. W. Ockwig, H. K. Chae, M. Eddaoudi, J. Kim, *Nature* **2003**, *423*, 705-714.

4 Y. L. Liu, V. C. Kravtsov, R. Larsen, M. Eddaoudi, *Chem. Commun.* **2006**, 1488-1490.

5 A. Kumar, S. S. Sun, A. J. Lees, *Coord. Chem. Rev.* **2008**, *252*, 922-939.

6 D. B. Amabilino, J. F. Stoddart, *Chem. Rev.* **1995**, *95*, 2725-2828.

7 M. E. Davis, *Top. Catal.* **2003**, *25*, 3-7.

8 B. Kesanli, W. B. Lin, *Coord. Chem. Rev.* **2003**, *246*, 305-326.

9 S. Leininger, B. Olenyuk, P. J. Stang, *Chem. Rev.* **2000**, *100*, 853-907.

10 B. Moulton, M. J. Zaworotko, *Chem. Rev.* **2001**, *101*, 1629-1658.

11 S. J. Lee, W. B. Lin, *Acc. Chem. Res.* **2008**, *41*, 521-537.

12 L. Dobrzanska, G. O. Lloyd, H. G. Raubenheimer, L. J. Barbour, *J. Am. Chem. Soc.* **2005**, *127*, 13134-13135.

13 L. Dobrzanska, G. O. Lloyd, H. G. Raubenheimer, L. J. Barbour, *J. Am. Chem. Soc.* **2006**, *128*, 698-699.

14 L. Dobrzanska, G. O. Lloyd, C. Esterhuysen, L. J. Barbour, *Angew. Chem., Int. Ed.* **2006**, *45*, 5856-5859.

15 L. Dobrzanska, G. O. Lloyd, T. Jacobs, I. Rootman, C. L. Oliver, M. W. Bredenkamp, L. J. Barbour, *J. Mol. Struct.* **2006**, *796*, 107-113.

16 L. Dobrzanska, G. O. Lloyd, L. J. Barbour, *New J. Chem.* **2007**, *31*, 669-676.

17 S. Takamizawa, E. Nakata, T. Saito, K. Kojima, *CrystEngComm* **2003**, *5*, 411-413.

18 S. Takamizawa, E. Nakata, T. Saito, *Angew. Chem., Int. Ed.* **2004**, *43*, 1368-1371.

19 S. Takamizawa, E. Nakata, T. Saito, T. Akatsuka, *Inorg. Chem.* **2005**, *44*, 1362-1366.

20 C. J. Kepert, *Chem. Commun.* **2006**, 695-700.

21 M. T. Kirchner, R. Boese, W. E. Billups, L. R. Norman, *J. Am. Chem. Soc.* **2004**, *126*, 9407-9412.

22 J. L. C. Rowsell, E. C. Spencer, J. Eckert, J. A. K. Howard, O. M. Yaghi, *Science* **2005**, *309*, 1350-1354.

23 E. C. Spencer, J. A. K. Howard, G. J. McIntyre, J. L. C. Rowsell, O. M. Yaghi, *Chem. Commun.* **2006**, 278-280.

24 D. G. Samsonenko, H. Kim, Y. Y. Sun, G. H. Kim, H. S. Lee, K. Kim, *Chem. Asian J.* **2007**, *2*, 484-488.

25 R. Matsuda, R. Kitaura, S. Kitagawa, Y. Kubota, R. V. Belosludov, T. C. Kobayashi, H. Sakamoto, T. Chiba, M. Takata, Y. Kawazoe, Y. Mita, *Nature* **2005**, *436*, 238-241.

26 R. Kitaura, S. Kitagawa, Y. Kubota, T. C. Kobayashi, K. Kindo, Y. Mita, A. Matsuo, M. Kobayashi, H. C. Chang, T. C. Ozawa, M. Suzuki, M. Sakata, M. Takata, *Science* **2002**, *298*, 2358-2361.

27 Y. Kubota, M. Takata, R. Matsuda, R. Kitaura, S. Kitagawa, K. Kato, M. Sakata, T. C. Kobayashi, *Angew. Chem., Int. Ed.* **2005**, *44*, 920-923.

28 Y. Kubota, M. Takata, R. Matsuda, R. Kitaura, S. Kitagawa, T. C. Kobayashi, *Angew. Chem., Int. Ed.* **2006**, *45*, 4932-4936.

29 A. Bondi, *J. Phys. Chem.* **1964**, *68*, 441-451.

30 G. M. Sheldrick, *Acta Crystallogr., Sect. A: Found. Crystallogr.* **2008**, *64*, 112-122.

31 F. H. Allen, O. Kennard, D. G. Watson, L. Brammer, A. G. Orpen, R. Taylor, *J. Chem. Soc. Perkin Trans. II* **1987**, S1-S19.

32 T. Steiner, A. M. Dasilva, J. J. C. Teixeiradias, J. Muller, W. Saenger, *Angew. Chem. - Int. Ed. Eng.* **1995**, *34*, 1452-1453.

33 J. L. Atwood, L. J. Barbour, A. Jerga, *Angew. Chem. Int. Ed.* **2004**, *43*, 2948-2950.

34 J. L. Atwood, L. J. Barbour, A. Jerga, B. L. Schottel, *Science* **2002**, *298*, 1000-1002.

35 A. L. Spek, *J. Appl. Cryst.* **2003**, *36*, 7-13.

36 D. Braga, F. Grepioni, *Angew. Chem., Int. Ed.* **2004**, *43*, 4002-4011.

37 D. Braga, S. L. Giaffreda, F. Grepioni, A. Pettersen, L. Maini, M. Curzi, M. Polito, *Dalton Trans.* **2006**, 1249-1263.

38 A. V. Trask, N. Shan, W. D. S. Motherwell, W. Jones, S. H. Feng, R. B. H. Tan, K. J. Carpenter, *Chem. Commun.* **2005**, 880-882.

39 J. Dillen, University of Stellenbosch (Stellenbosch), **2006**.

40 C. G. Marais, University of Stellenbosch (Stellenbosch), **2008**.

41 M. E. Brown, *Introduction to Thermal Analysis Techniques and Applications*, 2nd ed., Chapman & Hall, London, **2001**.

42 S. Vyazovkin, *Int. Rev. Phys. Chem.* **2000**, *19*, 45-60.

43 W. Gomes, *Nature* **1961**, *192*, 865-866.

44 M. E. Brown, A. K. Galwey, *Anal. Chem.* **1989**, *61*, 1136-1139.

45 K. Müller-Nedebock, University of Stellenbosch (Stellenbosch), **2008**.

46 A. J. Fletcher, K. M. Thomas, M. J. Rosseinsky, *J. Solid State Chem.* **2005**, *178*, 2491-2510.

47 S. Takamizawa, E. Nakata, *CrystEngComm* **2005**, *7*, 476-479.

48 B. L. Chen, S. Q. Ma, E. J. Hurtado, E. B. Lobkovsky, C. D. Liang, H. G. Zhu, S. Dai, *Inorg. Chem.* **2007**, *46*, 8705-8709.

49 S. Horike, D. Tanaka, K. Nakagawa, S. Kitagawa, *Chem. Commun.* **2007**, 3395-3397.

50 J. P. Zhang, X. M. Chen, *J. Am. Chem. Soc.* **2008**, *130*, 6010-6017.

51 A. D. Becke, *J. Chem. Phys.* **1993**, *98*, 1372-1377.

52 C. T. Lee, W. T. Yang, R. G. Parr, *Phys. Rev. B* **1988**, *37*, 785-789.

53 P. J. Stephens, F. J. Devlin, C. F. Chabalowski, M. J. Frisch, *J. Phys. Chem.* **1994**, *98*, 11623-11627.

54 J. T. H. Dunning, P. J. Hay, *Modern Theoretical Chemistry*, Plenum, New York, **1976**.

55 P. J. Hay, W. R. Wadt, *J. Chem. Phys.* **1985**, *82*, 299-310.

56 *Gaussian 03*, Revision B.05, Gaussian Inc., Wallingford CT, **2004**.

CHAPTER 5

SUMMARY AND GENERAL CONCLUSIONS

A systematic attempt to engineer the aperture size of the well-known clathrate of **1** is described in *Chapter 3*, with a view to producing a set of three porous systems with well-defined, but slightly different pore sizes. This afforded a chiral host framework with asymmetrical cavities that serve to order carbon tetrachloride molecules in a polar fashion throughout the material. Although not the aim of this particular study, this observation is unprecedented in the long history of inclusion studies of DC. Polar ordering of the guest occurs because the chiral clathrate cannot possess inversion symmetry, thus resulting in space group symmetry lowering of the system from the usual $R\bar{3}$ to $R3$. The significance of lowering the symmetry in this particular case is that it becomes possible to model the guest molecules in the cavities, whereas the usual $\bar{3}$ symmetry of DC and its thiol-analogue make this a difficult, if not impossible task. This result is highly relevant to the field of crystal engineering of channel inclusion compounds as non-linear optical materials. Although this new DC system did not yield a porous framework as was originally desired, studies of guest desorption and concomitant phase changes of clathrates $\mathbf{2}_{\mathbf{CCl4}}$ and $\mathbf{3}_{\mathbf{CCl4}}$ raised some fundamental questions about the mechanisms of guest desorption in organic inclusion compounds in general.

Chapter 4 describes the self-assembly of five isostructural molecular "hexagons" from different metal ions and the novel ligand 4,4′-bis(2-methylimidazol-1-ylmethyl)biphenyl (**L**). These metallocycles form molecular containers that are well-suited in size and shape for the study of small guest molecules that interact with one another, and with the surrounding host atoms. The guest transport processes could also be investigated to a certain extent, although further studies are warranted.

Results in this section include the identification of single-crystal to single-crystal transformations by compounds **13** and **14**, which transform from open (solvent-included) to collapsed metallocycles. The desorption processes of compounds **15** to

17 also occur as single-crystal to single-crystal transformations, but without collapse of the rings. This yielded three new related porous materials, each composed of Cd^{2+}, **L** and a halide X^- (where X = Cl, Br or I). An acetylene sorption isotherm was determined for **15** using a locally-constructed volumetric gas sorption device. Isotherms of CO_2 and N_2 sorption were also determined at different temperatures for **15-17**, but using a commercial gravimetric instrument. Together, these data provided sufficient information to demonstrate the influence of the halide (and hence the electrostatic profile of the cavity) on guest sorption ability. The most promising sorption ability for CO_2 and N_2 was shown by **15** (X = Cl), followed by **17** (X = Br) and then by **16** (X = I). Evidently, the increase in sorption efficiency corresponds with the increase in electronegativity together with a decrease in size of the halide counter ions.

As part of this study, a miniature gas cell was developed for the measurement of single-crystal diffraction data with the crystal exposed to a controlled pressure of any gas. This device proved to be highly beneficial for tracking structural changes during the step-wise uptake of gas by **15** with incrementally increasing pressure. Carbon dioxide and acetylene, two gasses of similar physical properties but contrasting quadrupole moments, were investigated in this manner. It was possible to elucidate structural detail with regard to gas:solid interactions and to observe even small structural changes in the host framework as gas was absorbed. Furthermore, by employing an electron count method (SQUEEZE), single-crystal intensity data could be used to determine sorption isotherms for the two gases – the ability to determine sorption isotherms for such small amounts of host material is unprecedented. The sorption profiles of the two gases differ only slightly, but the acetylene curve has an inflection that is not present in that for carbon dioxide. These slight differences in sorption behaviour could be rationalised on the basis of structural data, and are attributed to differences in host:guest interactions in addition to the specific manner in which the two gases are able to utilise the limited space provided by the host cavity. Sorption isotherm profiles were predicted using statistical mechanics together with parameters obtained from the single-crystal structures (structural deformation and energies of host:guest interactions). Upon scaling (pressure axis only) of these isotherms to match the experimental data, excellent agreement was obtained. The statistical mechanics model even accounts for the interesting inflection that is present

in the acetylene sorption isotherm, and the inflection is attributed to elastic coupling between neighbouring cavities. In contrast, only very slight deformation of the host accompanies the uptake of carbon dioxide sorption, and elastic coupling in this case is thus not a significant consideration. Other instances are commented on in which isotherm inflections were observed, but where satisfactory explanations were not provided by the authors.

A further interesting aspect of the study described in *Chapter 4* is that, although no apparent channels are present to link the discrete voids in the lattice, these materials readily sorb gas and solvent molecules. A possible explanation is that, as a result of thermally-induced atomic vibrations, openings between neighbouring voids occur spontaneously to form short-lived channels through which guest molecules can diffuse. This postulated mechanism of gas transport is supported by kinetic studies of CO_2 sorption of **15**, which imply that gas uptake follows a non-activated diffusion model. It is proposed that molecular mechanics simulations should be conducted in order to model diffusion of CO_2 and C_2H_2. This would be a complicated process involving two steps – i.e. the uptake of one molecule into an empty cavity, followed by uptake of a second molecule with concomitant realignment of the first molecule to accommodate the second. It would be interesting to compare the simulation of such a two-step process with that of a single-step process such as the sorption of the larger guests COS and CS_2.

The growing importance of crystal engineering to materials research cannot be overstated and is evidenced by the vast amount of literature on this subject that has appeared in recent years. Improved understanding of fundamental processes is key to the exploitation of crystal engineering for useful applications. Aspects that require further understanding include phenomena such as guest desorption from a host:guest β-phase to yield a porous β_0-phase. For example, what are the factors that influence host collapse in some cases and retention of the host morphology in others? Once we know more about these processes, can we exploit this knowledge in order to produce porous phases more reliably and also more frequently (*i.e.* since this is still a rare phenomenon)? This point is well illustrated by the structural rearrangement that occurs for the clathrates of **2** and **3** upon desolvation of the carbon tetrachloride guest, whereas the cadmium halide metallocycles of **15**, **16** and **17** exhibit desolvation

without rearrangement. It is intriguing to consider that these observations could be attributed to the greater solubility of the host in its guest in the case of the organic clathrates, as opposed to the rather low solubility of the metallocycles once they have formed.

Other important processes addressed in this work are (i) the diffusion (or transport) of relatively large guest molecules through seemingly nonporous crystals of compounds **15**, **16** and **17** and (ii) the two single-crystal to single-crystal transformations observed for compounds **13** to **14** that involve significant structural changes. Although the view once expressed by Ruzicka (i.e. that "… a crystal is a chemical cemetery")[1] has long been dispelled, a great deal still needs to be understood with regard to the dynamics in crystals. Continued efforts to explore these unexpected phenomena will provide the crystal engineer with more insight into the underlying processes governing the cooperativity in 'robust' crystals. Information such as this will lead the way towards reliably designing reversible transformation into 'soft' materials which can then be implemented as functional devices.

Finally, our approach of using an ensemble of complementary techniques for the study of CO_2 and C_2H_2 sorption by **15** (*i.e.* computational, gas sorption isotherms, single-crystal structure determinations under varied pressures and statistical mechanics) has afforded valuable information on the factors that influence physisorption. This emphasises the importance of systematic studies aimed at understanding of gas sorption processes. If we continue to pursue the answers to fundamental questions, we will lay the foundations of basic research that will ultimately enable us to rationally produce designer crystals for specific applications.

REFERENCE

1 J. D. Dunitz, V. Schomaker, K. N. Trueblood, *J. Phys. Chem.* **1988**, *92*, 856-867.

The attached CD contains:

Structural data relating to the final refinement of all single-crystal structures elucidated in this manuscript. Included files are '.hkl', '.RES' and the Crystallographic Information File (.CIF). Where appropriate the SQUEEZE output-file (.sqf) has also been included.

Gas sorption data for compounds **15**-**17**.

X-ray powder diffraction data for compounds **15**-**17** before and after gas sorption.

Publications, posters and talks.